Title

Improved transfection methods of primary cultured astrocytes for observation of cytoskeletal structures

Keywords

astrocytes, actin, ezrin, lasp-2, transfection

Authors

Chieko Ikoma[1], Kodai Inoue[1], Kouta Kasai[1], Satoko Tsukuda[1], Akiko Tamura[1], Shihoko Nakata[1], Yuto Iwata[1], Takumi Tamagawa[1], Ayako Nakayama[1], Kazunori Takano[1], Eiji Shigetomi[2,3], Shuichi Koizumi[2,3], Hiroyuki Nakagawa[4], and Asako G Terasaki[1]§

Authors' Affiliations and Addresses

1 Department of Biology, Graduate School of Science, Chiba University, Yayoicho, Inage-ku, Chiba 263-8522, Japan

2 Yamanashi GLIA Center, Interdisciplinary Graduate School of Medicine, University of Yamanashi, Chuo, 409-3898 Japan

3 Department of Neuropharmacology, Interdisciplinary Graduate School of Medicine, University of Yamanashi, Chuo, 409-3898 Japan

4 Division of Biology, Faculty of Science, Fukuoka University, Nanakuma, Jonan-ku, Fukuoka 814-0180, Japan

§ Author for correspondence (saki@faculty.chiba-u.jp)

Abstract

Astrocytes are the predominant type of glia in the central nervous system and have long branched stem processes and peripheral astrocyte processes (PAPs) contacting neurons and other glial cells. In many cell types, cell morphology and motility depend on actin cytoskeleton. However, a common astrocyte culture method in serum-containing medium generated undesired fibroblast-like cells; thus, the roles of cytoskeletal proteins in astrocyte morphology and motility have not been well studied. Previously, we reported a culture method of chicken astrocytes forming structures similar to stem processes and PAPs. In the current study, we improved transfection methods retaining astrocyte

morphology at low cell density, suitable for observing the behavior of proteins. Immunostaining and live imaging of plasma membrane-actin linking protein ezrin (a PAP marker) and another actin-binding protein lasp-2 (highly expressed in cultured astrocytes) demonstrated that our cultured astrocytes had microvillus protrusions, filopodia, lamellipodia, and focal adhesion-like elliptical structures, and the two proteins accumulated in different substructures. Our developed methods offer significant advantages for analyzing how astrocytes form stem processes and PAPs to access target cells.

Introduction

In the nervous system, neuronal function is maintained by various kinds of glial cells. Astrocytes are the predominant type of glia in the central nervous system (CNS). The term "astrocyte" is derived from stellate (aster, star-like) morphology with radial processes expressing intermediate filaments of glial fibrillary acidic protein (GFAP) observed in vivo. GFAP is a common astrocyte marker; in rodent brains, there are two main GFAP-positive astrocyte types: fibrous astrocytes organized along white matter tracts and protoplasmic astrocytes distributed relatively uniformly within cortical gray matter (reviewed by Ben Haim & Rowitch, 2016). Mature protoplasmic astrocytes in brain tissues comprise a cell body, several major branches from the cell body (referred as "astrocyte process", "stem processes", etc.), and perisynaptic or peripheral astrocyte processes (PAPs) that contact other cells. Some dyes, such as Lucifer yellow iontophoresis, can visualize whole astrocytes in tissues with bushy processes (Moye et al., 2019). Each astrocyte covers a large nonoverlapping territory with neighboring astrocytes (typically 50-100 μm diameter in mice and 100-400 μm in humans) (Oberheim et al., 2009), and each territory is thought to be a functional compartment (Endo et al., 2022). Historically, astrocyte morphological heterogeneity within brain areas of mammalian tissues has been reported, and this may be related to astrocyte functional heterogeneity.

Based on recent morphological studies, Baldwin et al., (2024) classified astrocyte processes into three categories that convey meaningful information about the particular astrocyte subcompartments. They suggested 'Branches' are the major stem processes emanating from the astrocyte soma, 'Branchlets' are the finer secondary structures emanating from branches, and 'Leaflets' are the thinner regions of astrocyte branches and branchlets that contact synapses. PAPs are known to regulate neuronal excitability and synaptic transmission via formation of tripartite synapses (reviewed by Semyanov & Verkhratsky, 2021). Astrocyte-neuron interactions also contribute to neural

development and differentiation (reviewed by Ben Haim & Rowitch, 2016). Astrocytes also enwrap layers of brain endothelial cells and form the blood-brain barrier with "endfeet", which are specialized distal extensions of astrocytes that contact the vasculature.Recently, astrocytes have been revealed to form astrocyte-oligodendrocyte and astrocyte-astrocyte interactions (reviewed by Yu & Khakh, 2022). Under light microscopy, PAPs are observed as ruffled lamellate processes and filopodia enriched in actin microfilaments.

During brain development, astrocytes arise from glial progenitors, disperse across cortical cell layers and columns, and increase region-specific morphological complexity (reviewed by Torres-Ceja & Olsen, 2022). Astrocytes also respond to CNS damage and disease, which involves morphological changes, including cell body hypertrophy and thickening of the major processes, along with actin and GFAP overexpression (reviewed by Lawrence et al., 2023). Astrocyte morphology is highly relevant to brain function and dysfunction. For example, territory areas of astrocytes were smaller in model mice of Huntington's disease, a severe neurodegenerative disease caused by a polyglutamine-encoding CAG expansion in the huntingtin (Htt) gene (Octeau et al., 2018). Also, in SAPAP3 knockout mice showing obsessive-compulsive disorder phenotypes, reduced territory sizes and disrupted actin cytoskeletal organization were observed (Soto et al., 2024).

In many cell types, adhesion, contraction, migration, and shape changes depend on actin cytoskeleton (reviewed by Svitkina, 2018). Various actin-binding proteins have been reported to control actin filament dynamics in the formation of actin-containing structures such as lamellipodia, filopodia, focal adhesions, and adherens junctions. Indeed, the actin-binding protein ezrin, connecting F-actin to cell membrane, was found to be localized at the neuropil of rat brain sections and microvillus protrusions of astrocytes immediately after dissociation (Derouiche & Frotscher, 2001; Haseleu et al., 2013). However, how actin-binding proteins regulate migration during development, branch emergence, PAP formation, enwrapping of synapses and connections with other glial cells have not been well examined. However, how the actin cytoskeleton of PAPs is regulated in the enwrapping of synapses and connections with other glial cells have not been well examined.

One reason for this is that astrocytes in vivo have complex 3D structures as described above. Another reason is the culture condition of primary astrocytes, which need to offer a more biologically relevant and accurate model and mimic in vivo functions. Morphologically intact astrocytes have been observed immediately after dissociation (Haseleu et al., 2013); however, a common method for culturing astrocytes in conventional Dulbecco's Modified Eagle Medium (DMEM) supplemented with fetal bovine serum (FBS) generated undesired fibroblast-like cells without stem processes (Aumann et al., 2017). Despite morphological differences, cultured fibroblast-like astrocytes

expressed GFAP and many astrocytic functions, such as metabolism, neurotransmission, and calcium signaling, were also observed in cultured cells (reviewed by Lange et al., 2012). Moreover, standard culture protocols using conventional medium recommend high cell density, which is unsuitable for observing cellular morphology (reviewed by Saura, 2007). Morphology and F-actin localization of fibroblast-like astrocytes are almost the same as that of fibroblasts, which have polygonal shape and thick stress fibers containing F-actin (Güler et al., 2021). Indeed, transcriptome analysis indicated that fibroblast-like astrocytes highly express hundreds of genes that are not normally expressed in astrocytes in vivo (Foo et al., 2011). Some studies indicated that PAPs of fibroblast-like astrocytes contained actin-binding proteins such as ezrin and profilin (details are described in discussion) (Lavialle et al., 2011; Molotkov et al., 2013). However, this was in reference to the thin membrane protrusions directly extending from the cell body as PAPs.

Thus, the factors that affect astrocyte morphology have been actively analyzed in tissues and animal models. Knockout or transgenic mice in which astrocytes change their morphology also provide information about specific genes. In living animals and tissues, adeno-associated viruses (AAVs) with astrocyte-specific promoters have been used as a powerful tool for transfecting genes into astrocytes (reviewed by Shigetomi et al., 2016). For example, AAVs utilizing shRNA of TrkB.T1, a brain derived neurotrophic factor (BDNF), reduced the volume and complexity of astrocytes in vivo (Holt et al., 2019). Moreover, AAVs utilizing proximity-dependent biotin identification (Bio-ID) have been used to elucidate protein-protein interactions (Soto et al., 2023). Recent RNA-seq findings have also provided extensive information. For example, putative actin-interacting proteins FERMT2 (FERM domain containing kindlin) and ezrin have been reported as astrocyte territory size-related modules based on analysis of RNA-seq and astrocyte volume in brain tissues (Endo et al., 2022). For uncovering the molecular basis of nanostructures of astrocytes in tissues and animals, electron microscopy provides high resolution protein localization; however the method requires the fixation of tissues. Two-photon microscopy or super-resolution microscopy (reviewed by Arizono et al., 2023) allows the monitoring of protein dynamics in living tissues. However, the methods are costly and furthermore, currently available imaging methods in living tissues are difficult for demonstrating protein dynamics.

Thus, the development of a cell culture system enabling high-resolution 2D observation is anticipated to facilitate knowledge sharing among researchers. Previously, we reported that a culture method of chicken astrocytes in Neurobasal medium containing b-FGF and B27 formed stem processes at low cell density. Lamellipodia and filopodia containing F-actin were observed in the cell periphery and specifically concentrated in stem process tips

(Tsukuda et al., 2019). However, localization of cytoskeletal proteins other than actin and GFAP has not been analyzed using immunostaining. Additionally, we have not observed behaviors of proteins because transfection methods that maintain these structures in cultured astrocytes have not been previously developed.

The current study has two main aims. First, we aimed to observe localization of cytoskeletal proteins in detail during the development of our cultured astrocytes. Additionally, we analyzed morphological heterogeneity regarding the number and length of branches, frequency of branching, and morphology of process tips. The second aim was to analyze the behaviors of actin-binding proteins in living astrocytes, whereby we examined various transfection methods (lipofection, electroporation, and lentivirus infection) that maintain stem processes and PAPs at low cell density that do not overlap with other cells. For preparing large quantities of homogeneous cells to examine various transfection conditions, we attempted to culture astrocytes that were directly cryopreserved after dissociation from the forebrain (directly cryopreserved astrocytes). In this study, to evaluate our culture method, we focused on the localization and behavior of two actin-binding proteins, ezrin and lasp-2. Ezrin is an anchor between actin and membrane, and is a well-studied standard PAP marker for analyzing astrocyte morphology (reviewed by Derouiche & Geiger, 2019). The other protein, lasp-2, has been reported to be localized in filopodia, lamellipodia, and focal adhesions in various types of cultured cells (reviewed by Butt & Raman, 2018). Localization of lasp-2 has not been studied in astrocytes, but high expression in astrocytes was confirmed in our previous study (Tsukuda et al., 2019). Thus, both proteins are used to examine whether localization varies across different actin-containing structures visualized by phalloidin-staining or fluorescent-tagged actin in cultured astrocytes.

The present study uses “stem process” for all processes observed in cultured astrocytes and follows Baldwin et al., (2024) in the use of the general terms “branches” and “branchlets” (see Fig. S1 for terminology). Baldwin et al., (2024) noted that truly “peripheral” astrocyte processes do not exist, because fine processes exist throughout astrocyte territories and “perisynaptic” astrocyte processes should be identified in processes specifically enwrapping synapses. However, in the present study, we use the term to describe the PAP-like structures observed in the cell periphery of cultured astrocytes because such structures contained ezrin, a PAP marker (see Fig. 3A-C, and E).

Results

Chicken astrocytes offer cell models mimicking the development and morphology of astrocytes in vivo

From the forebrain, approximately 5-10 × 10^5 dissociated cells per 15-day chick embryo were collected. The recovery rate of total cells (number of living and dead cells after thawing / total cell number after freezing) of the direct cryopreserved (DC) astrocytes after thawing was around 70%, and the viability of these cells was around 70%; thus, approximately 40–60% of the cryopreserved cells were culturable. As we described previously (Tsukuda et al., 2019), most contaminants, including erythrocytes, dead cell debris, and extracellular matrix, were removed after the first medium change on the next day. Storage of astrocytes in a deep freezer (-80°C) reduced both recovery rate and viability, with lower number of culturable cells (25-40% after 6 months, 15-25% after two years) and decreased proliferation rate. Liquid nitrogen retained cell viability for at least two years, similar to cells just after cryopreservation. Note that all data from freshly harvested (FH) and pre-cultured cryopreserved (PC) astrocytes for comparison with DC are from our previous study (Tsukuda et al., 2019).

First, we compared proliferation of DC astrocytes with FH and PC astrocytes at different initial cell densities (Fig. S2). The increase in coverage of DC astrocytes and PC astrocytes were slower than for FH astrocytes at all cell densities (Fig. S2A). At day 3 of culture, DC astrocytes and FH astrocytes showed similar rates of expression of glial fibrillary acidic protein (GFAP) as an index of differentiation, and PC astrocytes tended to show rather higher expression (Fig. S2B). At day 8 of culture, the GFAP-positive rate varied with density and culture method, but all remained above 70% in FH astrocytes and PC astrocytes and above 60% in DC astrocytes (Fig. S2B). There was no significant difference in morphology of DC astrocytes in phase-contrast images (Fig. S2C) and all DC astrocytes displaying more than 4 stem processes were GFAP-positive, as reported in FH astrocytes (Tsukuda et al., 2019) (data not shown).

Using staining with anti-GFAP antibody and phalloidin, the morphological differentiation of DC astrocytes (Fig. 1; see also Fig. S1 for terminology) was similar to that of FH astrocytes. When DC cells were cultured at an initial density of 0.1 × 10^5 cells/cm^2 (0.1id) for 3 days, short rod-shaped or Y-shaped cells under 100 μm in length were observed (Fig. 1, upper left). Some cells had stem processes (> 10 μm, arrowhead) and short protrusions (5-10 μm, square bracket), which directly extended from soma expected to grow into new branches and were strongly stained with phalloidin. About 45% of the cells expressed GFAP (Fig. S2B), but the staining was not filamentous but dotty. On day 5, 0.1id astrocytes generated multiple branches with GFAP staining stronger than on day 3 (Fig.1, upper middle). Some stem processes extended over 50 μm with collateral protrusions, emerging from the sides of stem processes and expected to grow into new branchlets (square brackets). All protrusions under 20 μm were stained with phalloidin but not anti-GFAP antibody. The longitudinal length of the cell area (covered with short branches and

branchlets) of some astrocytes extended over 100 μm. The width of process tips identified in phase-contrast images were varied, and both stick-like process tips (arrowheads, with process width < 2 times the branch/branchlet width) or larger palm-like process tips (arc, with process width > 2 times the branch/branchlet width) were stained with phalloidin. Collateral lamellipodia (dashed curly brackets), strongly stained with phalloidin, were observed on the sides of stem processes and were sometimes difficult to distinguish from lamellipodia directly extended from the cell body. On day 8, the coverage area of 0.1id astrocytes reached about 20% (Fig. S2A); most of the astrocytes were observed as isolated cells and palm-like process tips were observed more frequently (Fig. 1, upper right). Most stem processes over 10 μm were stained with the GFAP antibody and some astrocytes exhibited filamentous GFAP. The length and number of branches and branchlets radially increased, expanding their territories over 200 μm diameter until 7-10 days after plating (see Fig. 2). Their territories seemed to remain stable for at least 4 weeks, although new branching continued slowly.

Astrocytes cultured at initial densities of 0.2×10^5 cells/cm^2 (0.2id) after 3 days (Fig. 1, middle left) showed morphology similar to 0.1id cells after 5 days. On day 5, 0.2id astrocytes differentiated in a similar manner to 0.1id astrocytes after 8 days, and 0.2id astrocytes after 8 days exhibited filamentous GFAP more frequently than 0.1id astrocytes. Most of the 0.2id astrocytes formed exposed stem processes and some astrocytes were isolated, which is suitable for observing stem processes. Astrocytes cultured at 0.4×10^5 cells/cm^2 initial densities (0.4id) differentiated faster than 0.2id astrocytes, but coverage area reached 70% on day 8 (Fig. S2A; Fig.1, lower right).

As described previously (Tsukuda et al., 2019), contaminated epithelial-like cells, fibroblast-like cells, and neuronal inclusions were easily identified by their lack of GFAP staining as well as their strong polygonal phalloidin staining or long axons.

The morphology of GFAP-positive 0.1id and 0.2id astrocytes cultured for 8 days, which were considered to have finished territory expansion, were observed in detail with regards to the numbers and lengths of branches and branchlets, as well as the width of branches and palm-like structures at process tips (Fig. 2). Some astrocytes had thin and long branches over 50 μm without branchlets and all process tips were small (Fig. 2A), whereas some other astrocytes had thick branches less than 30 μm without branchlets and almost all process tips showed palm-like extension (Fig. 2B). Most astrocytes had multiple branches with various widths and formed many secondary/tertiary branchlets (Fig. 2C). Palm-like structures formed in the process tips were also varied in shape. Most tips had wavy peripherals accompanied with lamellipodia and filopodia (Fig. 2D, enlarged image a), although some tips were bumpy without filopodia (enlarged image b) and some tips had large bulges with long filopodia (enlarged image c).

The width of process tips varied from 5 μm to 30 μm. The territories of the cells, including stem processes and cell bodies, ranged from 50 μm to 300 μm in diameter (Fig. 2E), and branch numbers ranged from 3 to over 10.

Ezrin and lasp-2 are localized in different substructures of actin cytoskeleton of astrocytes

We compared the localization of two actin-binding proteins, ezrin and lasp-2, in DC astrocytes with specific antibodies. Ezrin localized in microvillus protrusions that extended from the cell periphery of astrocytes, which is difficult to identify in phase-contrast images. Collateral lamellipodia was always stained with anti-ezrin (Fig. 3A, dashed curly bracket), but the frequency of ezrin-positive protrusions in other structures varied among cells. In some cells, ezrin was concentrated in dense brush-like structures radially emerging from the palm-like process tips (Fig. 3A and 3B), but in some other cells, microvillus protrusions were sparsely distributed around the process tips (Fig. 3C). Microvillus protrusions directly emerged from stem processes were dense in specific areas (Fig. 3C and 3E) but sparse in other areas of the same processes (Fig. 3B, 3C, and 3F, double lines). Additionally, some GFAP-positive astrocytes hardly had microvillus staining with anti-ezrin (data not shown). The diameter of microvillus protrusions seemed to be uniform in all areas but the length varied up to 50 μm (e.g. Fig. 3E, long string-like structures indicated by open arrows). Phalloidin staining to visualize actin filaments weakly overlapped with ezrin staining, and this may be due to fewer filaments in microvillus protrusions than filopodia (Fig. 3C).

Lasp-2 was concentrated with F-actin in lamellipodia and filopodia at most process tips (Fig. 3D, dashed arcs and double arrowheads, respectively, in enlarged image a) and their colocalization was prominent in live cell imaging (described later in Fig. 4C and 5E). Lasp-2 was also observed in collateral protrusions, which are expected to be new branches or branchlets (Fig. 3D, square bracket). Magnified images of the process tips indicated that lasp-2 and actin colocalization at the base (inner part of tips) of lamellipodia and filopodia was observed, sometimes as elliptical structures of about 1-2 μm along the direction of branch extension (Fig. 3D, arrow in enlarged image a). Colocalization patterns of lasp-2 and actin were similar among astrocytes regardless of the length and width of their stem processes. In contrast, lasp-2 showed no colocalization with F-actin in all stress fiber-like structures (Fig. 3D, wedges in enlarged image b). There was no lasp-2 localization in ezrin-positive microvillus protrusions, and ezrin was not localized in collateral protrusions where lasp-2 was concentrated (Fig. 3E). Moreover, at most process tips, ezrin was not localized in the inner part of the tip where lasp-2 was concentrated as elliptical structures (Fig. 3F, arrows in enlarged image a). In a small part of the process tips, ezrin and lasp-2 showed colocalization as small dotty structure (Fig. 3F, asterisks in enlarged image b).

Improved method of electroporation visualizes behaviors of actin-binding proteins in living astrocytes

Using DC astrocytes, we examined transfection methods that retain astrocyte morphology at low cell density. Astrocytes cultured at initial density of 0.2-0.8 × 10^5 cells/cm^2 for 6-8 days in a 60-mm culture dish reached 40-80% coverage and generated 5-10 × 10^5 dissociated cells. Most of the cells tended to form colonies after electroporation. However, within 2 days of culture, all cells regenerated stem processes and some of the isolated cells with these structures were suitable for observation (Fig. 4A). Appropriate number of cells for transfection was about 0.4-0.8 × 10^6 and in cases where cell number was increased to the extreme (e.g. 2.0 × 10^6), transfection efficiency remained the same, although cells tended to form more colonies. Post-electroporation seeding cell density of ≤ 0.2 × 10^5 cells/cm^2 suppressed recovery of cell morphology and that of ≥ 0.8 × 10^5 cells/cm^2 resulted in fewer isolated astrocytes; about 20% of cells seemed to survive. The addition of a conditioned medium, which is thought to contain growth factors secreted by astrocytes, significantly accelerated morphological recovery. Moreover, the area of cell culture also affected the recovery. We initially attempted to culture electroporated astrocytes only in the small central glass portion of a glass-based dish (35-mm plastic dish with a centered 12 mm cover glass bottom), but found that astrocytes cultured in the entire dish base (including the plastic area) recovered faster. The 40-80% cell coverage before electroporation was adequate for both transfection efficiency and cell morphology, and cell morphology after transfection tended to deteriorate when the coverage was over 80% (Fig. 4A, upper panels).

About 5% of the electroporated cells expressed fluorescent-tagged proteins for visualizing actin and two actin-binding proteins, ezrin and lasp-2. Multiple plasmid vectors seemed to be electroporated simultaneously into the same cells; thus, transfection efficiencies of single plasmid and double plasmids with EGFP and mCherry tags were almost the same. Fluorescence was easily observed 1-4 days after electroporation and began to disappear 7 days after electroporation. We examined various culture durations before electroporation and found that shorter culture periods of less than 5 days required more days for formation of stem processes and PAPs, and culture periods of over 9 days suppressed recovery of morphology. We confirmed that electroporated cells with ≥ 4 stem processes were also GFAP-positive regardless of stem process length and process tip width (data not shown). After 4 days of transfection, in cells expressing mCherry-tagged proteins, large aggregates of fluorescent proteins were sometimes observed around the nucleus and they became more pronounced with culture length (Fig. 4C and 4D, open arrows), although localization of mCherry-tagged proteins in other areas was similar to that of EGFP-tagged proteins.

Fluorescent-tagged proteins showed almost similar localization patterns to immunostaining. EGFP-ezrin was

observed in the microvillus protrusions of uniform diameters on the cell surface, and co-transfected mCherry-actin was weakly observed in the protrusions (Fig. 4B, enlarged image b), similar to the phalloidin staining of actin (Fig 3C, enlarged image a). Ezrin was not colocalized with actin accumulated in process tips (Fig. 4B, enlarged image a). In contrast, transfected lasp-2 colocalized with actin accumulated in all process tips as well as in collateral protrusions of various widths, which may be areas where new branches form (Fig. 4C, square bracket). Magnified images of process tips indicated that lasp-2 was colocalized with actin in elliptical structures in a similar manner to immunostaining (Fig. 4C, arrows in enlarged images a and b). Cotransfection of EGFP-ezrin and mCherry-lasp-2 indicated that they were localized in different substructures of stem processes and process tips (Fig. 4D, enlarged image a and b). Kymographs of magnified images of stem processes also showed that substructures containing ezrin or lasp-2 actively moved, although colocalization was observed only in limited areas (asterisks in Fig. 4D').

In some cells transfected with pEGFP-Lifeact, a short peptide that binds to F-actin, relatively longer multiple filopodia and thick lamellipodia were observed in process tips more frequently both by electroporation and lipofection (Fig. S3B, double arrowheads and dashed arcs).

We also attempted lipofection of astrocytes with fluorescent-tagged plasmids following the manufacturer's protocol of cell lines in one-step transfection, only rod-shaped and spherical cells were observed (Fig. S3A). Reducing the reagents to one-fifth of the protocol (for example, 0.3 μL of transfection reagent for 1.0×10^5 cells) resulted in generation of stem processes, but most cells had less than 4 processes. Two-step transfection generated astrocytes with multiple stem processes more frequently, but it was difficult to observe localization of fluorescent proteins because the manufacturer's protocol required 80-90% confluency. Conditioned medium significantly promoted morphological recovery of the astrocytes in two-step transfection at lower cell density (Fig. S3A); however, the number and length of the stem processes in fluorescent-positive astrocytes were lower than those following electroporation (S3B, left). The transfection efficiency of lipofection was about 5-10%. Seven days of culture post-thawing is appropriate for transfection, and 3 days post-transfection is appropriate for observation, with fluorescence beginning to fade after around 1 week post-lipofection.

Lentivirus vectors allow long-term observation of actin-binding proteins in astrocytes

In contrast to electroporated astrocytes that were dissociated from dishes, lentivirus infection hardly affected astrocyte development (Fig. 5A), although some cell debris was observed post-infection (Fig. 5B, phase contrast image). We confirmed that infection efficiency was around 10-50%, and this efficiency was similar at cell densities

up to 80% and between 3 to 7 days of culturing. Fluorescence derived from the fluorescent-tagged vectors, which may be integrated into the genome, were observed even at 28 days of culturing (data not shown). Cell morphology was disrupted up to 2 days post-lentiviral infection, but gradually recovered after day 3. Similarly, fluorescence was weak up to day 2, but could be observed from day 3. Astrocytes infected with lentiviral vectors expressing EGFP, EGFP-lasp-2, and mCherry-lasp-2 had well-maintained morphology of stem processes and process tips compared with lipofection and electroporation (Fig. 5B-5D). In contrast to electroporation (which incorporates multiple plasmid types simultaneously), in lentiviral infection, cells were independently infected with two lentivirus vectors containing EGFP and mCherry tags, respectively; thus, it was difficult to observe cells infected with both vectors (1-5%).

Using lentiviral infection, control EGFP was found to be uniformly distributed in the cytoplasm (Fig. 5B). In contrast, lasp-2 was concentrated in protrusions from the soma as well as process tips, which is similar to the observations from immunostaining and electroporation (Fig. 5C, square bracket, arrowheads, and arcs). In the process tips, small elliptical structures (1-2 μm) at the base of filopodia and lamellipodia were also observed (Fig. 5C, arrows in enlarged images a and b). Live imaging showed that lamellipodia and filopodia containing EGFP-lasp-2 were actively moving, and elliptical structures also appeared and disappeared (Supplemental Movie 2). We confirmed that localization and fluorescence maintenance period of the mCherry-lasp-2 lentivirus were the same as those of the EGFP-tagged lentivirus (Fig. 5D). In some cells infected with mCherry-tagged proteins using lentivirus, aggregates of fluorescent proteins were sometimes observed in a similar manner to mCherry-tagged proteins in electroporated cells (Fig. 5D, open arrow). Sara Fluor 497 actin-probe, an F-actin–binding small molecule, strongly stained F-actin in filipodia and lamellipodia at process tips and was colocalized with mCherry-lasp-2 (Fig. 5E, double arrowheads and dashed arcs). Sara Fluor 497 actin-probe also stained elliptical structures where lasp-2 accumurated (Fig. 5E, arrows in enlarged image a).

To observe the behavior of actin-binding proteins during elongation of stem processes, we observed time-lapse imaging of lasp-2, which was concentrated in process tips in immunostained, electroporated, and infected cells. Astrocytes were infected with a lentiviral vector of control EGFP or EGFP-lasp-2 on day 3 of culture and then observed on day 5, when cells are expected to be expanding their territories. Fluorescent images and phase contrast images were acquired every 2 hours using a glass bottom dish with a grid to detect the positions of the cells (Fig. 5F, see analysis method in Fig. S4).

Stem processes of astrocytes sometimes extended, retracted, and disappeared frequently. Most process tips of extending stem processes had palm-like structures, and the retracting stem processes had small tips (Fig. 5F, control,

a and b; lasp-2, a). Sometimes, a tip split into two and then fused back (Fig. 5F, lasp-2, b and b'). Moreover, some collateral protrusions developed into new branchlets (Fig. 5F, control, b') and some collateral protrusions disappeared (Fig. 5F, lasp-2, c). Phase contrast images indicated extension and branching of stem processes occurred despite remaining attached to other cells (Fig. 5F, control, b'). Compared with the control EGFP, EGFP-lasp-2 was concentrated in the process tips of extending stem processes and newly developed collateral protrusions (Fig. 5F, lasp-2, a at 0, 4, 6, 8 h; b at 2, 4, 8 h). Relative to extending stem processes, fluorescence intensity of EGFP-lasp-2 at process tips decreased in retracting stem processes (Fig. 5F, lasp-2, a at 2 h; b at 6 h).

Discussion

Understanding how neurons and glial cells develop, maintain, and change their elaborate morphology is essential for analyzing neural networks. To achieve this, primary cell culture is a powerful tool, and both a culture method mimicking cell function (including morphology) and a method for transfecting vectors are essential. In primary neurons, established protocols succeeded in high resolution 2D observation of protein localization in neurons that spontaneously generate growth cones, develop axons, and form mature cells with elaborate dendrite morphologies. In neurons, actin-binding proteins play essential roles in the motility of growth cones, which drive axonal development and formation of spines interacting with neurons and astrocytes (reviewed by Lowery & Van Vactor, 2009; Gallo, 2024). Development of the stunning complexity and cell-cell interactions via PAPs of astrocytes also involves extensive cytoskeleton remodeling. However, very little is known about the molecular machinery behind these comprehensive shapeshifts of astrocytes (reviewed by Schiweck et al., 2018). As mentioned in the introduction, a key reason contributing to this limited insight is that the cultured astrocyte models do not accurately recapitulate astrocytes in situ or during normal morphogenesis. Purification protocols of rodent astrocytes consisting of several negative immunopanning steps to remove other cell types and positive immunopanning to collect astrocytes have been developed, and the purified astrocytes formed stem processes in serum-free medium at low cell density (Foo, 2013). However, immunopanning requires many kinds of antibodies, of which specificity should be confirmed for the species.

Here, we describe an improved, highly reproducible, and cost-effective protocol for preparation and transfection of chicken astrocytes. From cell coverage area and GFAP staining, we confirmed that directly cryopreserved

astrocytes, suitable for accumulating large quantities of homogeneous cells, differentiated similarly to both freshly harvested astrocytes and pre-cultured cryopreserved astrocytes, and were used for subsequent experiments (Fig. 1 and Fig. S1 and S2). Although our culture contained GFAP-negative cells (Fig. S2), we confirmed cells with 4 or more stem processes were GFAP-positive astrocytes (Fig. 1 and 2) and used these cells with rich stem processes for analysis. Directly cryopreserved astrocytes showed heterogeneity in branch and branchlet numbers as well as PAP morphology (Fig. 2 and 3), suggesting that our cultured astrocytes much more closely resemble in vivo astrocytes. Kálmán (1998) describes the distribution of GFAP in the brain of chickens from hatching to maturity and found that astrocyte morphology and territories differed among areas in the forebrain. Although territory size was not explicitly measured, the study's figures indicate that territories extended 50-500 μm along the long axis, and our observations that some cultured astrocytes extended their territories to up to 300 μm fit within this range.

Chickens have been used extensively as research models for developmental studies and as resources for protein purification and primary cultured cells. Low costs, accessibility, ease of manipulation, availability of detailed descriptions of morphogenesis and whole genome sequences (Smith et al., 2023), and recently developed genetic engineering techniques (Panda & McGrew, 2022) have made chickens a robust model for developmental research. Many actin-binding proteins, including lasp-2 analyzed in our study, have been purified from chicken tissues and their amino acid sequences show high similarity to those of mammals. As an example of lasp-2, our previous research indicated that amino acid similarity between chickens and humans is over 90% (Fujita et al., 2021). Moreover, dating as far back as a decades earlier, the function of actin-binding proteins have been analyzed in chicken primary fibroblasts, myoblasts, cardiocytes, and sensory neurons, of which morphology and motility were confirmed to mimic cells in vivo (Geiger, 1979; Endo et al., 2007; Zieseniss et al., 2008). Due to the adequate replication of in vivo cells, our cultured chicken astrocyte system will be a vital resource for neuroscience research.

Our culture mimicking astrocyte morphology provided high-resolution 2D observation of stem processes and PAPs, albeit with lower stem process complexity. This simpler complexity makes it suitable for analyzing how stem processes extend their territories and form branches, and how PAPs contribute to stem process elongation and cell-cell interactions. Additionally, measurements of cell area and number of branches and branchlets in 2D systems are much easier than in 3D systems. Thus, our system is suitable for analyzing the effects of knockdown or overexpression of some proteins, as well as drugs, which are reported to affect the morphology of astrocytes in animals. Moreover, 2D culture systems are applicable for analysis of cell-substrate structures using e.g. total internal reflection fluorescence microscopy (TIRFM) and interferometric photoactivated localization microscopy (iPALM)

(reviewed by Kanchanawong & Calderwood, 2023). Recently, it has been revealed that the cell-cell adhesion between neurons and astrocytes depends both on direct binding via cell-adhesion molecules (CAMs) and indirect binding via extracellular matrix (reviewed by Saint-Martin & Goda, 2022), and our culture system could be applied to co-culture systems to observe such interactions. We also consider that previous studies of actin-binding proteins utilizing cultured fibroblast-like astrocytes could elucidate more information if they were to adapt our newly established protocols. As an example, a study in fibroblast-like astrocytes indicating that formation of PAPs (referred as thin membrane protrusions directly emerged from cell body) require ezrin in the membrane/cytoskeleton-bound form (Lavialle et al., 2011). Another study indicated that overexpression of mutant profilin affected the number and length of PAPs, which are also observed as thin membrane protrusions of fibroblast-like astrocytes (Molotkov et al., 2013). Such studies could adapt our protocols to elucidate the full mechanisms of how actin-binding proteins regulate formation of stem processes and PAPs.

Using vectors coding actin-binding proteins (ezrin and lasp-2) to observe actin cytoskeleton in living astrocytes, we optimized transfection protocols and successfully improved two of three protocols (electroporation and lentivirus infection) that retained astrocyte morphology at low cell density. Electroporation is easy and suitable for high-throughput analysis of multiple proteins identified by large scale analysis such as RNA-seq and Bio-ID, although the number of completely isolated cells are lower relative to lentiviral infection (Fig. 4 and Fig. 5). In contrast, lentivirus infection is a more complex approach but adequately retains cell morphology (Fig. 5); thus, this method will be beneficial for analyzing protein functions in detail. We observed that Lifeact affected filopodia length and lamellipodia thickness (Fig. S3B) and recent reports have raised concerns about Lifeact-associated artefacts (Flores et al., 2019); thus, we used EGFP/mCherry-actin for visualizing the whole actin cytoskeleton (G-actin and F-actin)(Fig. 4B and 4C). Additionally, we confirmed that actin probes were useful to visualize actin cytoskeleton with actin-binding proteins (Fig. 5E). Ezrin and lasp-2 localization in transfected cells were similar in both live imaging and immunostaining; thus, we conclude that our directly cryopreserved astrocytes and improved transfection protocols are suitable for investigating the roles of actin-binding proteins in astrocytes.

In this study, various actin-containing structures were observed in our cultured astrocytes. F-actin stained with phalloidin always accumulated in both short protrusions from soma during early culture stages and in collateral protrusions emerged from branches or branchlets, indicating that the formation of stem processes and branching depends on actin cytoskeleton (Fig. 1). Collateral lamellipodia densely stained with phalloidin indicated that cultured astrocytes have active ruffles similar to those observed in vivo (Fig. 1, dashed brackets). Accumulation of F-actin

was observed in process tips, which varied in shape, indicating that elongation of stem processes also depends on actin cytoskeleton (Fig. 2D and 3D). Thin stress-fiber-like structures in our cultured astrocytes (indicated with wedges in Fig. 1-3) were markedly different from the thick stress-fiber-like structures previously observed in fibroblast-like astrocytes that contained a high activation state of myosin-II (John, 2004). However, extending stem processes may depend on tension of stress-fiber-like structures because they extended along stem processes. Some cell types have stress fibers with discontinuous localization of mechanosensing proteins, such as zyxin and nonmuscle myosin, that make up the contractile apparatus (reviewed by Smith et al., 2014). The irregular and stronger staining of F-actin in stress-fiber-like structures may be related to the irregular localization of such proteins, and thus, future research should analyze their localization.

Microvillus protrusions on the cell periphery, stained with phalloidin and anti-ezrin, seemed to mimic protrusions of PAPs because ezrin is known to be a PAP marker in vivo (Fig. 3A-C and E). These protrusions were difficult to identify in phase-contrast images in our cultured astrocytes, but anti-ezrin staining indicated that astrocytes may interact with other cells over a wide area (Fig. 3A). The frequency of ezrin-rich microvillus protrusions varied among cells and areas in our cultured astrocytes, suggesting that ezrin locally controls cell-cell interactions. The diameter of microvillus protrusions in astrocytes seemed to be uniform in all areas, suggesting that the protrusions have similar structure observed in intestinal brush borders, which have uniform diameters. Electron tomography indicated that each microvilli in intestinal brush borders has a regular number of actin filaments between 30-40 (Ohta et al., 2012); thus, the number of actin filaments in astrocyte microvillus structures may be regulated in the same manner.

In contrast to ezrin-staining, anti-lasp-2 antibody consistently stained short protrusions that directly emerged from soma, collateral protrusions, collateral lamellipodia, and process tips, indicating that lasp-2 always bind to F-actin in these structures (Fig. 3D-F). Additionally, elliptical structures containing lasp-2 and F-actin (arrows in Fig. 3D-F) observed both in immunostaining and live imaging might be cell-substrate adhesions because lasp-2 has been reported to be localized in focal adhesions in some cell lines (Nakagawa et al., 2009). However, cell-substrate adhesions of astrocytes have not been well examined apart from the localization of paxillin in fibroblast-like astrocytes (Güler et al., 2023) and the expression and localization of focal adhesion components in brain tissues, both of which have not been analyzed in-depth. Thus, whether any components of focal adhesions like paxillin show colocalization with lasp-2 in the elliptical structure should be investigated. Anti-lasp-2 did not stain ezrin-positive microvillus protrusions and, vice versa, anti-ezrin did not stain lasp-2 positive structures, suggesting that lasp-2 and ezrin localized in different substructures of actin cytoskeleton (Fig. 3E and 3F).

Live cell imaging of astrocytes transfected with fluorescent-tagged vectors expressing actin, ezrin, and lasp-2 revealed that filopodia, lamellipodia, and microvillus protrusions are actively moving structures (Fig. 4, 5, Supplemental Movie 1 and 2). We found that stem processes of astrocytes sometimes extended, retracted, and disappeared frequently. Axonal elongation of neurons commonly continues until growth cones come in contact with other cells, so the movement of stem processes are somewhat different from neurons. Extension of stem processes of astrocytes is also different whereby extensions that remain attached to other cells are continuous (Fig. 5F). We observed lasp-2 and actin concentrated in filopodia and lamellipodia as well as in focal adhesion-like elliptical structures in extending process tips; we also observed lasp-2 and actin dissociated from retracting tips. These observations support the idea that both proteins were concentrated in cell-substrate contacts and control the mobility of astrocytes through the extracellular matrix.

Using a BioID AAV vector infected in rat brains to label proteins that localized closely to ezrin, Soto et al. (2023) identified over 100 proteins including the gene product of LASP2/NEBL, which generates lasp-2 and another actin-binding protein nebulette as splice isoforms. Since mRNA of nebulette and lasp-2 is mainly expressed in cardiac tissues and in the brain (Terasaki et al., 2004; Zieseniss et al., 2008), respectively, the gene product is considered to be lasp-2. They also indicated that staining of brain sections expressing EGFP-ezrin using anti-nebulette C-terminal antibody (with shared sequence with lasp-2) showed colocalization within the astrocyte territory. Combining their findings in whole cell images with our findings using more detailed observations of actin-containing structures under high resolution, it is supposed that both ezrin and lasp-2 localized in actin-rich structures on the cell surface of astrocytes, but lasp-2 mainly controls the formation of lamellipodia and filopodia along with cell-substrate adhesion, whereas ezrin mainly controls cell-cell contact via microvillus protrusions formed on lamellipodia or protrusions that directly emerged from stem processes. To understand the function of lasp-2 in the elongation and cell-substrate adhesions of stem processes in more detail, it is necessary to transfect deletion constructs of lasp-2 (lacking actin-binding regions or adhesion sites to components of focal adhesions) into astrocytes using actin probes to determine how they function with or without actin in process tips. Ezrin-containing microvillus protrusions were sometimes concentrated in the process tips (Fig. 3A-C, E), and this may support stem process elongation in some cases. This idea is also supported by a report that GFAP-positive astrocytes in nervous system-specific ezrin knockout mice had satellite morphology, whereas ezrin-deficient astrocytes revealed altered cell morphology and reduced volume (Schacke et al., 2022). Additionally, astrocyte-specific depletion of ezrin resulted in shorter astrocyte leaflets and reduced astrocyte contact with the synaptic cleft (Badia-Soteras, 2023).

The morphology of palm-like process tips with highly motile lamellipodia and filopodia, as well as the concentration of actin and actin-binding proteins (ezrin and lasp-2) observed in this study, are similar to those of neuronal growth cones (Fig. 4C, D, and 5B-E) although extending and retracting behaviors are different (Fig. 5F). Moreover, in oligodendrocytes, it has been suggested that process tips are structurally and functionally similar to growth cones (reviewed by Thomason et al., 2020). During development, astrocytes may extend their processes with each other and with other glial cells, and form complex neural networks with neurons. The morphology of glial cells and neurons is highly relevant to the function and dysfunction of the brain (reviewed by Wilson et al., 2023). The disruption of cell-cell interactions between astrocytes and neurons was also reported in many diseases (reviewed by Blanco-Suárez et al., 2017). In neurons, several actin-binding proteins were reported to be responsible for neuronal migration disorders, and many actin-binding proteins are involved in neuronal disorders and cancers (reviewed by Liu, 2011). Similar mechanisms related to actin-binding proteins may be revealed in morphologically abnormal astrocytes observed in brain disease pathogenesis, and recent studies suggested actin-based morphological improvements of astrocytes, as described in the introduction (Endo et al., 2022; Soto 2024). Thus, analysis of functions of numerous actin-binding proteins in astrocytes using our developed methods may lead to the restoration of such abnormalities and could partly ameliorate disease.

In summary, we have described astrocytes in our cultured method that form various structures containing actin cytoskeleton in a similar manner to cells in vivo. Additionally, improved astrocyte transfection protocols permit easy observation of protein behavior. Our improved protocols for preparing chicken astrocytes and transfection methods offer numerous benefits in cell culture, including low costs and reproducibility of functional test results. Indeed, our detailed observation of localization and behavior of ezrin and lasp-2 revealed that each actin-containing structure may comprise different actin-binding proteins. The methods developed in the present study offer significant advantages for filling in the knowledge gaps regarding protein activities in vitro and the roles of their coding genes analyzed in tissues and animal models, thereby contributing to future astrocyte research.

Materials and methods

Antibodies

For immunostaining, Cy3-labeled anti-GFAP monoclonal antibody (clone G-A-5, 1:4000, Sigma-Aldrich, St. Louis,

MO, USA), anti-lasp-2 specific polyclonal antibody immunoabsorbed with lasp-1 (1:5; Terasaki et al., 2004), and anti-ezrin monoclonal antibody (clone 3C12, 1:50, Santa Cruz Biotechnology, Dallas, TX, USA) were used for primary antibodies. Alexa Fluor 488-labeled and Alexa Fluor 546-labeled anti-rabbit and anti-mouse IgG antibodies (1:500 or 1:1000, Thermo Fisher, Waltham, MA, USA) were used for secondary antibodies. Alexa Fluor 488-labeled and rhodamine-labeled phalloidin (0.066 μM, Thermo Fisher) were used for F-actin staining. Hoechst 33342 (0.1 μg/mL, Sigma-Aldrich) was used for nuclear staining.

Fluorescent protein expression vectors

pEGFP vectors coding chicken lasp-2 were prepared as described previously (Terasaki et al., 2004). pEGFP-lifeact were prepared with the insertion of Lifeact oligo DNA, a 17 amino acid peptide of yeast actin binding protein ABP140 (Riedl, 2008). pEGFP-human beta actin was purchased from Clontech (Mountain View, CA, USA). pEGFP vector coding human ezrin were purchased from Addgene (cat. no. 20680, MA, USA). To generate pmCherry-lasp-2, BamHI-EcoRI fragments of pEGFP-lasp-2 were subcloned into the BamHI and EcoRI sites of a pmCherry-C1 vector (Clontech). To generate pmCherry-actin, the XhoI-BamHI fragment of pEGFP-actin was subcloned into the XhoI and BamHI site of a pmCherry-C1 vector. All plasmids for electroporation and lipofection were prepared with the Nucleobond Xtra Midi EF (Macherey-Nagel, Düren, Germany).

To generate lentivirus vectors expressing EGFP-lasp-2 and mCherry-lasp-2, the region coding fluorescent-tagged proteins were amplified by PCR using PrimeSTAR Max (Takara, Shiga, Japan), following manufacturer's protocol. The forward primer to amplify each protein was agaagacaccgactctagaggatccCTACCGGTCGCCACCATG (lowercase indicates primer region for subcloning into the BamHI site and uppercase indicates primer region for connecting the region from CMV promoter to the first methionine of EGFP and mCherry). Reverse primers to amplify cDNA of each protein were as follows: EGFP-lasp-2 and mCherry-lasp-2 : tgtaatccagaggttgattgtcgacTGGGGAATTCGGACTAGAGAC (lowercase indicates primers for subcloning into the SalI site and uppercase indicates primers for stop codon of lasp-2). The regions coding EGFP of the pLenti CMV EGFP Puro (658-5) vector (Addgene) were removed using BamHI and SalI and replaced with PCR products using NEBuilder HiFi DNA Assembly (New England BioLabs, MA, USA).

Preparation of chick forebrain astrocytes

Astrocytes were prepared from 15-day-old embryonic chick forebrains, following our previous study (Tsukuda et al.,

2019). Briefly, cerebral meninges and superficial blood vessels were removed in phosphate-buffered saline (PBS), and cells were dissociated with 0.1% trypsin-EDTA (WAKO, Tokyo, Japan) for 15 min. Dulbecco's Modified Eagle Medium (DMEM) containing 10% FBS or calf serum (CS) was added to inactivate trypsin, and cells were then filtered through Kimwipes (Kimberly-Clark, Irving, TX, USA) in a Swinnex filter holder (Merck Millipore, Burlington, MA, USA).Dissociated cells were washed three times by DMEM containing 10% FBS or CS. After the final wash, total cell number in the medium was counted and precipitated cells were dissolved in Cell Banker 1 plus (ZENOAQ, Tokyo, Japan) at 3.2×10^6 cells/mL and stored in liquid nitrogen until use.

Cell culture

FH cells and cells cultured for 2–3 days and then cryopreserved (pre-cultured cryopreserved astrocytes) were cultured as previously described (Tsukuda et al., 2019); see detailed protocol). For the culture of DC astrocytes, cells in cryotubes were thawed using water at 37°C and washed with DMEM twice. 0.2% Trypan Blue Solution (Sigma-Aldrich) was used as a cell stain to assess cell viability. Cells for immunostaining were plated on a 35-mm culture dish with circular coverslips of 15 mm diameter (Matsunami, Tokyo, Japan). Cells for electroporation or one-step lipofection were plated on a 35-mm culture dish. Cells for lentivirus infection or two-step lipofection were plated on a 35-mm glass base dish (D11140H, Matsunami). Cells for time-lapse imaging were plated on a 35-mm glass base dish with grid (grid size 150 μm) (IWAKI, Tokyo, Japan). All dishes were coated with 0.08 mg/mL Poly-L-Lysine (Sigma-Aldrich) and cell densities were varied in experiments (described later). The culture medium was the same as in Tsukuda et al. (2019): Neurobasal medium (Thermo Fisher) supplemented with 2% B-27 supplement (Thermo Fisher), 0.5 mM L-glutamine, 25 μM Glutamax (Thermo Fisher), and 5 ng/mL b-FGF (WAKO). On the next day after plating, the medium was replaced completely by fresh medium following vigorous pipetting. Half of the medium was changed approximately twice a week.

Cells were imaged using inverted microscopy (CK40, Olympus, Tokyo, Japan) equipped with a digital camera (L-835, Hozan, Osaka, Japan) at 20× magnification. The percentage of area covered by cells at various proliferation stages were manually determined following our previous study (Tsukuda et al., 2019).

Immunocytochemistry

Astrocytes cultured on coverslips were fixed with 4% formaldehyde in PBS for 5 min at 37°C, and permeabilized with 0.1% Triton-X100 and 10% goat serum in PBS, for 30 min at room temperature. Nonspecific background

staining was reduced with signal enhancer (Thermo Fisher) or Blocking One Histo (Nacalai, Kyoto, Japan). For GFAP staining, the cells were stained with Cy3-labeled anti-GFAP antibody diluted in Signal Enhancer HIKARI(Nacalai) for 2 h at room temperature. For lasp-2 and ezrin staining, the cells were stained with primary antibodies overnight at 4°C, then rinsed with PBS, and stained with secondary antibodies for 1 h at room temperature. For observation of F-actin and nucleus, cells were stained with fluorescent labeled-phalloidin and Hoechst 33342 for 10 min. Finally, the cells were mounted on slide glasses using SlowFade Gold antifade reagent (Thermo Fisher).

Following our previous study (Tsukuda et al., 2019), GFAP expression rates were determined from the number of cells identified by nuclear staining with Hoechst 33342 as well as the number of GFAP-expressing cells identified by anti-GFAP antibody staining. Three randomly selected images from each experiment were analyzed.

Fluorescence microscopy

Cells were observed using an Axiovert135 inverted fluorescence microscope (Carl Zeiss, Oberkochen, Germany) equipped with ×40 phase-contrast objective lens or ×63 DIC lens, fluorescence filters (Zeiss 39, 38HE, and 43HE), and a Coolsnap HQ charge-coupled device (CCD) camera (Teledyne Photometrics, Tucson, AZ, USA) operated by the IPLab software (Scanalytics, Billerica, MA, USA), or an inverted fluorescence microscope (Axiovert135) equipped with fluorescence filters (Zeiss 15 and 17) and a Retiga R1 CCD camera (Teledyne Photometrics) operated by the Micro-Manager.

Electroporation

Astrocytes cultured at densities of 0.2-0.8 × 10^5 cells/cm^2 in 60 mm dishes for 6-8 days (50-80% coverage) were transfected with fluorescent-tagged vectors (pEGFP-actin, pmCherry-actin, pEGFP-lifeact, pEGFP-ezrin, and/or pmCherry-lasp-2) by electroporation using NEPA21 (Nepagene, Chiba, Japan). Medium was collected from the cell culture dishes and stored as conditioned medium. Next, the cells were washed with PBS twice and treated with 0.25% trypsin-EDTA (WAKO) for 2 min. DMEM containing 10% FBS was then added to inactivate trypsin and the cells were detached by pipetting. Cells (0.4-0.8 × 10^6) were transferred to microtubes, supernatants were carefully removed, and then a mixture of two types of plasmids (1.0-2.5 μg each) and Opti-MEM (Thermo Fisher) was added. The cell mixture was transferred to a NEPA 2 mm cuvette and voltage was applied. The parameters were set to the following values: poring pulse (voltage: 275.0 V; pulse length: 0.3 msec; pulse interval: 50.0 msec; number of pulses: 2; decay rate: 10%; polarity: +), transfer pulse (voltage: 20.0 V; pulse length: 50.0 msec; pulse interval: 50.0 msec; number of

pulses: 5; decay rate: 40 %; polarity: +/−). After electroporation, the cells were plated on 35-mm glass base dishes (D11140H, Matsunami) coated with 0.08 mg/mL Poly-L-Lysine at cell densities of 0.2-0.6 × 10^5 cells/cm^2 and cultured in Neurobasal medium containing half of the conditioned medium. Transfected cells were observed between 2 to 5 days after electroporation, and the medium was not changed during observation.

Lipofection

Lipofection was performed according to the manufacturer's method, except the amounts of transfection reagent and plasmids were adjusted. Astrocytes cultured at densities of 0.2-0.9 × 10^5 cells/cm^2 for 2-7 days were transfected with fluorescent-tagged vectors (pEGFP-lifeact and pmCherry) by lipofection using ScreenFect A (WAKO) in two different ways.

One-Step Transfection: Cells were washed with PBS twice and treated with 0.25% trypsin-EDTA (WAKO) for 2 min. DMEM containing 10% FBS was then added to inactivate trypsin and the cells were detached by pipetting. Cells (0.3-0.9 × 10^5) were transferred to microtubes, suspended in antibiotic-free Neurobasal medium, and a mixture of plasmid and ScreenFect TMA Reagent (WAKO) was added. After the one-step lipofection, the cells were plated on 35-mm glass bottom dishes coated with 0.08 mg/mL Poly-L-Lysine and cultured in antibiotic-free Neurobasal medium.

Two-Step Transfection: Medium was collected from the cell culture dishes and stored as conditioned medium in 4°C. Next, cells were washed with PBS once and then a mixture of antibiotic-free medium, plasmid, and ScreenFect TMA Reagent was added. The medium was replaced completely by conditioned medium on the next day after two-step lipofection.

Lentivirus infection

pLenti-EGFP, pLenti-EGFP-lasp-2, and pLenti-mCherry-lasp-2 were transfected into 293FT cells with psPAX2 (Addgene cat. no. 12260) and pCMV-VSV-G (Addgene cat. no. 8454) using PEI MAX (Polysciences, Warrington, PA, USA) at 40 μg/μL, pH 7.1 to produce virus particles. 293FT cells were cultured in DMEM with 10% FBS, 100 units/mL penicillin, 0.1 μg/μL streptomycin, and 200 mM L-glutamine. 293FT cells cultured in a 75 cm^2 culture flask for 4 days until 50-90% coverage was replaced with antibiotic-free DMEM and then a mixture of Opti-MEM (Thermo Fisher), PEI MAX, and plasmids was added. After the mixture was reacted for 4-12 h, the medium was replaced with DMEM with antibiotics. After 3 days of culturing, medium (virus particle solution) was collected and filtered using

a 0.45 μm pore filter unit (Merck Millipore, Darmstadt, Germany) to avoid contamination of 293FT cells. Virus solutions were stored in cryotubes in liquid nitrogen, thawed under running water, and used for subsequent infections. Astrocytes cultured for 3 to 7 days were transfected with fluorescent-tagged vectors (pLenti-EGFP, pLenti-EGFP-lasp-2, and pLenti-mCherry-lasp-2) by lentivirus infection. From each cultured astrocyte dish containing 2 mL of medium, 1 mL or the entire volume of medium was removed; then, 2 mL of virus solution in DMEM added 2% B27 and 5 ng/mL bFGF was added. The day after infection, the medium was replaced entirely with Neurobasal medium with antibiotics. For live imaging of F-actin of infected astrocytes, SaraFluor 497 actin probe (HMRef)(Goryo Kayaku, Hokkaido, Japan) was added to the medium at final concentration of 100 nM and observed immediately.

Time-lapse imaging

Astrocytes cultured on a 35-mm glass dish with 150 μm grid (IWAKI) at a density of 0.2×10^5 cells/cm^2 for 3 days were transfected with fluorescent-tagged vectors (EGFP and EGFP-lasp-2) by lentivirus infection. Time-lapse images were taken 2 to 4 days after infection. Phase-contrast images and fluorescence images of isolated astrocytes were captured every 2 h up to 8 h. The phase-contrast images of the grid in the same area were captured to monitor the location and elongation of astrocytes. Each binarized fluorescence image of astrocytes was overlaid on a grid image for subtraction of cell area and to create images of the grid excluding cell areas. Next, each subtracted grid image was superimposed onto the respective fluorescence astrocyte image to create fluorescence images with grids. Finally, the fluorescence images with grids were aligned in the same position according to the grid in order to monitor the location and elongation of astrocytes (Fig. S4).

Statistical analyses

All data are expressed as mean ± standard error of mean (SEM) obtained from at least four independent experiments. "N" refers to the number of independent experiments.

FIGURE LEGENDS

Fig. 1. Representative images of astrocytes at different initial cell densities

Representative images of direct cryopreserved astrocytes stained with anti-GFAP antibody (red), phalloidin (green),

and Hoechst 33342 (blue) at different initial cell densities after 3, 5, and 8 days. Examples of "Protrusions directly emerged from soma"/"Collateral protrusions" (square brackets), "Collateral lamellipodia" (dashed curly brackets), "Stick-like process tips" (arrowheads), and "Palm-like process tips" (arcs), as described in Fig. S1, are indicated only in the top panels. Wedges indicate irregular and stronger staining of F-actin in stress-fiber-like structures. All figure annotations, except arrows, open arrows, and double arrowheads, apply to subsequent figures. Scale bar = 20 μm; areas highlighted by the squares are magnified, with scale bar = 5 μm (same scales apply to fluorescent images in subsequent figures).

Fig. 2. Heterogeneity of cultured astrocytes

Cultured astrocytes with various morphologies. Cells were cultured for 8 days and stained with the same antibodies and reagents as in Fig. 1. (A) Astrocyte displaying thin branches with stick-like process tips (arrowheads) without branchlets; (B) astrocyte showing thick branches with palm-like process tips (arcs) and collateral lamellipodia (dashed curly bracket); (C) astrocyte showing multiple branches of various widths with many secondary/tertiary branchlets; (D) astrocyte with variable morphology of process tips; (E) astrocyte with territory of diameter over 100 μm.

Fig. 3. Localization of ezrin and lasp-2 in cultured astrocytes

Representative immunostaining images of (A, B) ezrin (green) and GFAP (red) after 11d; (C) ezrin (green) and F-actin (red) after 10d; (D) lasp-2 (green) and F-actin (red) after 7d; (E, F) lasp-2 (green) and ezrin (red) after 7d. Double arrowheads and dashed arcs indicate filopodia and lamellipodia, respectively. Doubled lines in (B), (C), and (F) indicate examples of areas where anti-ezrin is hardly stained. Open arrows indicate long string-like structures stained with anti-ezrin. Arrows in (D), (E), and (F) indicate elliptical structures stained with anti-lasp-2. Asterisks in (F) indicate examples of structures where lasp-2 and ezrin colocalized. Brightness of some enlarged images were enhanced to visualize fine structures (same adjustments apply to fluorescent images in subsequent figures).

Fig. 4. Morphology of astrocytes transfected by electroporation and localization of fluorescent-tagged proteins

(A) Lower magnification view of astrocytes cultured at high density (initial cell density of 0.6×10^5 cells/cm^2; cultured for 7 days) and low density (initial cell density of 0.3×10^5 cells/cm^2; cultured for 6 days). Phase contrast images show cells just before trypsin treatment (pre-transfection) and cultured for one day after electroporation.

Scale bar = 200 μm. (B-D) Representative images of (B) EGFP-ezrin and mCherry-actin, (C) EGFP-actin and mCherry-lasp-2, and (D) EGFP-ezrin and mCherry-lasp-2 at 2, 3, and 2 days post-transfection, respectively. See supplementary movie 1 for (D); (D') kymographs of magnified segment of stem process surface from supplemental movie 1 with a sequence interval of 20 sec. Arrows in (C) and (D) indicate examples of elliptical structures of fluorescent-tagged lasp-2. Asterisks in (D') indicate examples of structures where lasp-2 and ezrin colocalized.

Fig. 5. Morphology of astrocytes infected with lentivirus and localization of fluorescent-tagged proteins

(A) Lower magnification view of astrocytes before and after (1d, 2d and 5d) infection. Scale bar = 200 μm. (B-E) Representative images of (B) EGFP, (C) EGFP-lasp-2, (D) mCherry-lasp-2, and (E) mCherry-lasp-2 and added Sara Fluor 497 actin probe in astrocytes at 7, 4, 6, and 5 days post-infection with lentivirus vectors, respectively. (F) Time-lapse imaging of astrocytes infected with lentiviral coding with EGFP or EGFP-lasp-2 every 2 hours. Arrows in (C) to (E) indicate examples of elliptical structures of fluorescent-tagged lasp-2.

DETAIL PROTOCOLS

Materials

Preparation of medium

DMEM with FBS was prepared by mixing the following reagents:

・DMEM	88 mL
・Fetal Bovine Serum	10 mL (10%)
・200mM L-glutamine	2 mL (4 mM)
・penicillin (10^5 unit / mL)	0.1 mL（100 unit/mL）
・streptomycin (100 mg / mL)	0.1 mL（0.1 mg/mL）
Total	Approx. 100 mL

Neurobasal medium with supplements was prepared by mixing the following reagents:

・Neurobasal medium（Thermo Fisher 21103-049）	49 mL
・200 mM L-glutamine	0.125 mL（0.5 mM）
・200 mM Glutamax (Thermo Fisher 35050-038)	6.25 μL （25 μM）
・penicillin（10^5 unit/mL）	0.05 mL（100 unit/mL）
・streptomycin（100 mg/mL）	0.05 mL（0.1 mg/mL）
・B27 supplement（Thermo Fisher 17504-044）	1 mL（2%）
・10 μg/mL b-FGF (WAKO 064-04541)	0.025 mL（5 ng/mL）
Total	Approx. 50 mL

B27 supplement and b-FGF should be added just before use.

Preparation of 0.08 mg/mL Poly-L-Lysine (PLL):

・Poly-L-lysine hydrobromide（SIGMA P2636, mol wt 30,000-70,000）

1. Add PBS to the bottle containing PLL to make 0.8 mg/mL solution.
2. Mix well by pipetting and collect it in a 50-mL conical tube.
3. For sterilization, filter the solution into a new tube using a 0.22 μm filter.
4. Aliquot 1 mL portions into 15 mL conical tubes, and store at -20°C.
5. At time of use, prepare a 0.08 mg/mL solution by adding 9 mL of sterile PBS (-) to the aliquot.

※ 0.08 mg/mL PLL can be stored at 4°C for up to 2 weeks.

Preparation of coverslips:

Circular coverslips of 15 mm diameter used in immunostaining were prepared using the following steps.

1. Place 100 pieces of coverslips in a 500-mL glass beaker, add 100 mL of nitric acid, and allow to stand for more than 2 h (stir once every 30 minutes).
2. Remove the nitric acid and rinse the coverslips under running tap water for more than 2 h.
3. Rinse the coverslips with deionized water stirring with tweezers for more than 1 h (change water at least 10 times during the process).
4. Rinse the coverslips 3 times with 50 mL of 100% ethanol.
5. Soak the coverslips overnight in 100% ethanol.
6. Rinse the coverslips once with 50 mL of 100% ethanol.
7. Dry the coverslips in a laminar flow cabinet and store in a case.
8. On the day the cells are cultured, put three coverslips in a 35-mm culture dish and coat with 2 mL of 0.08 mg/mL Poly-L-Lysine for more than 2 h.

Preparation of directly cryopreserved astrocytes:

・Autoclave two Swinnex® filter holders (Merck Millipore, Burlington, MA, USA) inserted with two sheets of Kimwipes (Kimberly-Clark, Irving, TX, USA) and one Swinnex® filter holder with four sheets of Kimwipes.

・Incubate fertilized chicken eggs in the humidified egg incubator at 37.7 °C for 15 days.

1. Set up two 60-mm empty dishes and four 60-mm dishes with PBS.
2. Sterilize eggs (containing chicken embryos) with 70% ethanol. Make a small hole on each of the shells with the back end of tweezers.
3. Gently pick up the chicken embryo with tweezers and transfer to the first empty dish. Repeat for remaining embryos.
4. Decapitate the embryo with the tweezers and transfer only the heads to the second empty dish. Repeat for the remaining embryos.
5. Peel off the hairy skin and remove the skulls to expose the forebrains using the tweezers. Repeat for remaining embryos.
6. Pull out all hemispheres of the forebrains with bent-tip tweezers and transfer them to the first dish with PBS. After gently shaking the hemispheres to remove blood in the first dish with PBS, transfer all hemispheres to the second dish with PBS.
7. In the second dish with PBS, remove the cerebral meninges with blood vessels (thin semi-translucent elastic membranes) using tweezers under a stereomicroscope, and transfer the forebrains to the third dish with PBS.
8. In the third dish containing PBS, tear the hemispheres in half, ensuring that no cerebral meninges remain, and transfer to the fourth dish containing PBS.
9. Transfer all hemispheres to one 50-mL conical tube containing 6 mL of PBS and tear them into 1-2 mm pieces with tweezers.
10. Add 4 mL of 0.25% trypsin-EDTA to make 0.1% trypsin and incubate at 37°C for 15 min. Mix by inversion once every 5 min.
11. Centrifuge the forebrain suspension at 700 rpm for 3 min.
12. Remove the supernatant, add 10 mL of DMEM with FBS, and mix by inversion.
13. Centrifuge the forebrain suspension at 700 rpm for 3 min.
14. Remove the supernatant, add 12 mL of DMEM with FBS, and dissociate cells from forebrain tissues by pipetting 30 times using a 10-mL disposable pipette.
15. Filter the forebrain suspension with a Swinnex® filter holder with two sheets of Kimwipes connected to a 10-mL syringe. Change the holder when the flow decreases (two holders are commonly used to filter suspension from six embryos).
16. Repeat the filter process again but using four sheets of Kimwipes instead.

17. Centrifuge the filtrate at 1200 rpm for 3 min.
18. Remove the supernatant, add 8 mL of DMEM with FBS, and resuspend by pipetting several times.
19. Centrifuge the cell suspension at 1200 rpm for 3 min.
20. Repeat steps 18-19 twice.
21. Remove the supernatant, add 8 mL of Neurobasal medium with supplements, and resuspend by pipetting.
22. Count the cell number with a hemocytometer.
23. Centrifuge the cell suspension at 1000 rpm for 5 min.
24. Remove the supernatant and resuspend the cells in Cell Banker 1 plus at 32×10^5 cells/mL.
25. Dispense the cells in cryotubes at 8, 16, or 32×10^5 cells/tube and store in liquid nitrogen until use.

Thawing and culture of directly cryopreserved astrocytes:

1. Coat the culture dishes or culture dishes with coverslips (for immunostaining) with 2 mL of 0.08 mg/mL Poly-L-Lysine for more than 2 h.
2. Wash the dishes 2 times with PBS. Keep the dish in a 37°C incubator.
3. Defrost cells in cryotubes using a beaker of 37°C water.
4. Transfer thawed cells (in Cell Banker 1 plus) to a 15 mL tube containing DMEM (10 times the volume of Cell Banker 1 plus).
5. Centrifuge the cell suspension at 1000 rpm for 5 min.
6. Remove the supernatant, add 2 mL of DMEM with FBS, and resuspend by pipetting.
7. Centrifuge the cell suspension at 1000 rpm for 5 min.
8. Remove the supernatant, add 1 mL of Neurobasal medium with supplements, and resuspend by pipetting.
9. Count the cell number with a hemocytometer.
10. Adjust the cell suspension to the desired cell density using Neurobasal medium with supplements and place on cell culturing dishes (2 mL for 35-mm dish and 3 mL for 60-mm dish).
11. The next day, to dissociate contaminants (dead cells, erythrocytes, and extracellular matrix) from the culture dish, vigorously pipette the culture medium with 1-mL disposable pipette for 10-20 times [cells remain adhered to dish].
12. Remove the culture medium and immediately replace it with fresh Neurobasal medium with supplements.

13. Change half the Neurobasal medium with supplements every 3 or 4 days. Pipetting to dislodge contaminants is not required.

Electroporation:

1. Coat a 35-mm glass base dish for culture of transfected cells with 2 mL of 0.08 mg/mL Poly-L-Lysine for more than 2 h and then wash the coated dish with 1 mL of PBS twice. Keep the dish aside for later (step 9).
2. Set the NEPA21 parameters.
3. Mix 20 µL of Opti-MEM and 1.0-2.5 µg of plasmids in a 1.5-mL microtube.
4. Collect all the medium from the cell culturing dish and store in a 15-mL centrifuge tube at 37°C (referred as conditioned medium).
5. Wash the cells with 2 mL of PBS twice.
6. Add 1.5 mL of 0.25% trypsin-EDTA and observe under microscopy to ensure that the cells are detached.
7. Add 1.5 mL of DMEM to the dish, resuspend by pipetting several times, and transfer to a 15-mL conical tube.
8. Add 1.5 mL of DMEM again to the dish, resuspend by pipetting several times, and transfer to the same 15-mL conical tube.
9. Centrifuge the cell suspension at 1000 rpm for 5 min. Meanwhile, add 1 mL of Neurobasal medium and 1 mL of conditioned medium to the PLL-coated dish (set aside for step 19).
10. Remove the supernatant from the centrifuged sample, add 2 mL of DMEM, and resuspend by pipetting several times.
11. Centrifuge the cell suspension at 1000 rpm for 5 min.
12. Remove the supernatant, add 1 mL of Neurobasal medium, and resuspend by pipetting.
13. Count the cell number using a hemocytometer.
14. Transfer 4.0-6.0 × 10^5 cells to a 1.5-mL microtube.
15. Centrifuge the microtube at 1000 rpm for 10 min.
16. Remove all the supernatant carefully using a micropipette.
17. Add the mixture of Opti-MEM and plasmids (from step 3) and resuspend by pipetting several times.
18. Transfer the mixture to a NEPA 2 mm cuvette using a micropipette to prevent foaming and then apply voltage.

19. Add a small amount of medium removed from the PLL-coated dish (from step 9) to the cuvette using a NEPA dropper.
20. Transfer the cell suspension in the cuvette to the PLL-coated dish using the NEPA dropper and incubate at 37°C.

Lipofection:

One-Step Transfection:

1. Coat a 35-mm glass base dish for culture of transfected cells with 2 mL of 0.08 mg/mL Poly-L-Lysine for more than 2 h and then wash the coated dish with 1 mL of PBS twice.
2. Collect all the medium from the cell culturing dish and store in a 15-mL conical tube at 4°C (referred as conditioned medium).
3. Wash the cultured cell with 1 mL of PBS twice.
4. Add 1 mL of 0.25% trypsin-EDTA and observe under microscopy to ensure that the cells are detached.
5. Add 1 mL of DMEM to the dish, resuspend by pipetting several times, and transfer to a 15-mL conical tube.
6. Add 1 mL of DMEM again to the dish, resuspend by pipetting several times, and transfer to the same 15-mL conical tube.
7. Centrifuge the cell suspension at 1000 rpm for 5 min.
8. Remove the supernatant, add 1 mL of antibiotic-free Neurobasal medium, and resuspend by pipetting.
9. Count the cell number using a hemocytometer.
10. Transfer 0.3-0.9 × 10^5 cells to a 1.5-mL microtube.
11. Prepare another two 1.5-mL microtubes containing 15 μL of Dilution buffer.
12. Add 25-600 ng of plasmid to one of the microtubes.
13. Add 0.15-1.8 μL of ScreenFect TMA Reagent to the other microtube (ensure the Reagent is vortexed well before use).
14. Combine the plasmid and Reagent solutions, mix immediately by pipetting 10 times, and allow to stand at room temperature for more than 5 min for complex formation.
15. Add the mixture to the microtube containing cells and mix gently by pipetting several times.
16. Transfer the cell suspension in the microtube to a PLL-coated glass base dish and incubate at 37°C.

Two-step Transfection:

1. Prepare two 1.5-mL microtubes containing 15 μL of Dilution buffer.
2. Add 25-600 ng of plasmid to one of the microtubes.
3. Add 0.15-1.8 μL of ScreenFect TMA Reagent to the other microtube (vortex the Reagent well before use).
4. Combine the plasmid and Reagent solutions, mix immediately by pipetting 10 times, and allow to stand at room temperature for 15-20 min for complex formation.
5. Collect all the medium from the cell culturing dish and store in a 15-mL conical tube at 4°C (referred as conditioned medium).
6. Wash the cells with 2 mL of PBS once.
7. Add 1 mL of antibiotic-free Neurobasal medium to the mixture of plasmid and Reagent.
8. Add this mixture to the cell culturing dish and gently shake the dish to mix.
9. Add 1 mL of antibiotic-free Neurobasal medium to the cell culturing dish.
10. The next day, replace the entire medium with the conditioned medium warmed to 37°C.

Lentivirus infection:

(Must be performed in a Biosafety Level 2 laboratory)

1. Thaw the virus in cryotubes under running water.
2. Remove all or 1 mL of the medium from the cell culturing dish.
3. Add 0.2, 1, or 2 mL of virus solution to the dish and incubate at 37°C.
4. The next day, replace the entire medium with Neurobasal medium containing antibiotics.

Generation of overlay images of fluorescence images and phase-contrast grid images:

(All steps were performed using ImageJ; see Fig. S4)

1. Capture fluorescence images of the cells (A) along with phase-contrast images of the grid of the glass-bottom dishes (B) at different optical foci but in the same area.
2. Open one phase-contrast image of the grid (B); then, to extract all grid line edges (yellow) within the image, use Wand Tool to click on black grid lines [at the appropriate tolerance setting] (C).
3. Save the extracted grid edges of using 'ROI manager' (C).
4. Keep the window of ROI settings open, and then open the cell fluorescence image and generate a binarized fluorescence image of the cells using 'Threshold' (D).
5. Extract the extracellular areas of the binarized fluorescence image from (D) using Wand Tool and save these areas in the same ROI setting window using 'ROI manager' (E).
6. Select the two ROI saved in steps 3 and 5 in the same 'ROI manager' window, and superimpose using the AND command in 'ROI manager' (More > AND) to generate grid edge images subtracted with cell area [yellow lines] (F). Arrow in (F) indicates the area of the cell overlapping with the grid that is removed.
7. Select the phase-contrast image with the grid excluding cell areas generated in step 6 and copy (Edit > Copy), and then open the fluorescence image (A) again and paste (Edit > Paste) onto this image, to create a fluorescence image with the grid (G).
8. Save the image generated in step 7 as a new tif file (H).
9. Adjust the positions of fluorescence images captured every 2 h by rotation and cropping according to the grid so that the images at each time are in the same position. The corresponding phase-contrast images of the cells can be created in the same manner of rotation and cropping as the fluorescence images (see Fig. 5F).

Acknowledgments

We thank Professor Baljit Khakh for the discussions and suggestions on terminology used in this paper.

Competing interests

The authors declare no competing interests.

Author contributions

Conceptualization: C.I., K. I., H.N., A.G.T.; Methodology: C.I., K.I., K.K., S.T., A.T., S.N., Y.I., T.T., K.T., A.N.,

A.G.T.; Formal analysis: C.I., K.I., K.K., T.T.; Investigation: C.I., K.I., K.K., S.T., A.T., S.N.,.; Resources: A.N., K.T., H.N.; Data curation: C.I., K.I., K.K.; Writing - original draft: C.I., A.G.T.; Writing - review & editing: E.S., A.G.T.; Visualization: C.I., K.I., K.K., T.T; Supervision: E.S., K.S, A.G.T.; Project administration: A.G.T.; Funding acquisition: A.G.T.

Funding

This work was supported by JSPS KAKENHI grant number 19570066 and Initiative for Realizing Diversity in the Research Environment of the Chiba University.

Academic English Consultation in Chiba University supported English editing.

Data availability

All relevant data and supplementary information can be found within the article and our previous paper (Tsukuda et al., 2019).

References

Arizono, M., Idziak, A., Quici, F., & Nägerl, U. V. (2023). Getting sharper: the brain under the spotlight of super-resolution microscopy. *Trends in Cell Biology*, *33*(2), 148–161. https://doi.org/10.1016/j.tcb.2022.06.011

Aumann, G., Friedländer, F., Thümmler, M., Keil, F., Brunkhorst, R., Korf, H. W., & Derouiche, A. (2017). Quantifying Filopodia in Cultured Astrocytes by an Algorithm. *Neurochemical Research*, *42*(6), 1795–1809. https://doi.org/10.1007/s11064-017-2193-0

Badia-Soteras, A., Heistek, T. S., Kater, M. S. J., Mak, A., Negrean, A., van den Oever, M. C., Mansvelder, H. D., Khakh, B. S., Min, R., Smit, A. B., & Verheijen, M. H. G. (2023). Retraction of Astrocyte Leaflets From the Synapse Enhances Fear Memory. *Biological Psychiatry,* *94*(3), 226–238. https://doi.org/10.1016/j.biopsych.2022.10.013

Baldwin, K. T., Murai, K. K., & Khakh, B. S. (2024). Astrocyte morphology. *Trends in Cell Biology*, *34*(7), 547–565. https://doi.org/10.1016/j.tcb.2023.09.006

Ben Haim, L., & Rowitch, D. H. (2016). Functional diversity of astrocytes in neural circuit regulation. *Nature Reviews Neuroscience*, *18*(1), 31–41. https://doi.org/10.1038/nrn.2016.159

Blanco-Suárez, E., Caldwell, A. L. M., & Allen, N. J. (2017). Role of astrocyte–synapse interactions in CNS disorders. *Journal of Physiology*, *595*(6), 1903–1916. https://doi.org/10.1113/JP270988

Butt, E., & Raman, D. (2018). New frontiers for the cytoskeletal protein LASP1. *Frontiers in Oncology* (Vol. 8, Issue SEP, pp. 1–11). https://doi.org/10.3389/fonc.2018.00391

Derouiche, a, & Frotscher, M. (2001). Peripheral astrocyte processes: monitoring by selective immunostaining for the actin-binding ERM proteins. *Glia*, *36*(3), 330–341. http://www.ncbi.nlm.nih.gov/pubmed/11746770

Derouiche, A., & Geiger, K. D. (2019). Perspectives for ezrin and radixin in astrocytes: Kinases, functions and pathology. *International Journal of Molecular Sciences*, *20*(15). https://doi.org/10.3390/ijms20153776

Endo, F., Kasai, A., Soto, J. S., Yu, X., Qu, Z., Hashimoto, H., Gradinaru, V., Kawaguchi, R., & Khakh, B. S. (2022). Molecular basis of astrocyte diversity and morphology across the CNS in health and disease. *Science*, *378*(6619). https://doi.org/10.1126/science.adc9020

Endo, M., Ohashi, K., & Mizuno, K. (2007). LIM kinase and slingshot are critical for neurite extension. *The Journal*

of Biological Chemistry, *282*(18), 13692–13702. https://doi.org/10.1074/jbc.M610873200
Flores, L. R., Keeling, M. C., Zhang, X., Sliogeryte, K., & Gavara, N. (2019). Lifeact-GFP alters F-actin organization, cellular morphology and biophysical behaviour. *Scientific Reports*, *9*(1), 1–13. https://doi.org/10.1038/s41598-019-40092-w
Foo, L. C. (2013). Purification of rat and mouse astrocytes by immunopanning. *Cold Spring Harbor Protocols*, *8*(5), 421–432. https://doi.org/10.1101/pdb.prot074211
Foo, L. C., Allen, N. J., Bushong, E. A., Ventura, P. B., Chung, W. S., Zhou, L., Cahoy, J. D., Daneman, R., Zong, H., Ellisman, M. H., & Barres, B. A. (2011). Development of a method for the purification and culture of rodent astrocytes. *Neuron*, *71*(5), 799–811. https://doi.org/10.1016/j.neuron.2011.07.022
Fujita, Y., Chokki, T., Nishioka, T., Morimoto, K., Nakayama, A., Nakae, H., Ogasawara, M., & Terasaki, A. G. (2021). The emergence of nebulin repeats and evolution of lasp family proteins. *Cytoskeleton*, *78*(9), 419–435. https://doi.org/10.1002/cm.21693
Gallo, G. (2024). The Axonal Actin Filament Cytoskeleton: Structure, Function, and Relevance to Injury and Degeneration. *Molecular Neurobiology*, *61*(8), 5646–5664. https://doi.org/10.1007/s12035-023-03879-7
Geiger, B. (1979). A 130K Protein from Chicken Gizzard : Its Localization at the Termini of Microfilament Bundles in Cultured Chicken Cells. *Cell*, *18*(1), 193–205. https://doi.org/10.1016/0092-8674(79)90368-4
Güler, B. E., Krzysko, J., & Wolfrum, U. (2021). Isolation and culturing of primary mouse astrocytes for the analysis of focal adhesion dynamics. *STAR Protocols*, *2*(4). https://doi.org/10.1016/j.xpro.2021.100954
Güler, B. E., Linnert, J., & Wolfrum, U. (2023). Monitoring paxillin in astrocytes reveals the significance of the adhesion G protein coupled receptor VLGR1/ADGRV1 for focal adhesion assembly. *Basic and Clinical Pharmacology and Toxicology*, *133*(4), 301–312. https://doi.org/10.1111/bcpt.13860
Haseleu, J., Anlauf, E., Blaess, S., Endl, E., & Derouiche, A. (2013). Studying subcellular detail in fixed astrocytes: dissociation of morphologically intact glial cells (DIMIGs). *Frontiers in Cellular Neuroscience*, *7*(May), 1–10. https://doi.org/10.3389/fncel.2013.00054
Holt, L. M., Hernandez, R. D., Pacheco, N. L., Torres Ceja, B., Hossain, M., & Olsen, M. L. (2019). Astrocyte morphogenesis is dependent on BDNF signaling via astrocytic TrkB.T1. *ELife*, *8*, 1–27. https://doi.org/10.7554/eLife.44667
John, G. R. (2004). Interleukin-1 Induces a Reactive Astroglial Phenotype via Deactivation of the Rho GTPase-Rock Axis. *Journal of Neuroscience*, *24*(11), 2837–2845. https://doi.org/10.1523/JNEUROSCI.4789-03.2004
Kálmán, M., Székely, A. D., & Csillag, A. (1998). Distribution of glial fibrillary acidic protein and vimentin-immunopositive elements in the developing chicken brain from hatch to adulthood. *Anatomy and Embryology*, *198*(3), 213–235. https://doi.org/10.1007/s004290050179
Kanchanawong, P., & Calderwood, D. A. (2023). Organization, dynamics and mechanoregulation of integrin-mediated cell-ECM adhesions. *Nature Reviews Molecular Cell Biology volume, 24*(February). https://doi.org/10.1038/s41580-022-00531-5
Lange, S. C., Bak, L. K., Waagepetersen, H. S., Schousboe, A., & Norenberg, M. D. (2012). Primary cultures of astrocytes: Their value in understanding astrocytes in health and disease. *Neurochemical Research*, *37*(11), 2569–2588. https://doi.org/10.1007/s11064-012-0868-0
Lavialle, M., Aumann, G., Anlauf, E., Pröls, F., Arpin, M., & Derouiche, A. (2011). Structural plasticity of perisynaptic astrocyte processes involves ezrin and metabotropic glutamate receptors. *Proceedings of the National Academy of Sciences of the United States of America*, *108*(31), 12915–12919. https://doi.org/10.1073/pnas.1100957108
Lawrence, J. M., Schardien, K., Wigdahl, B., & Nonnemacher, M. R. (2023). Roles of neuropathology-associated reactive astrocytes: a systematic review. *Acta Neuropathologica Communications*, *11*(1), 1–28. https://doi.org/10.1186/s40478-023-01526-9
Liu, J. S. (2011). Molecular genetics of neuronal migration disorders. *Current Neurology and Neuroscience Reports*, *11*(2), 171–178. https://doi.org/10.1007/s11910-010-0176-5
Lowery, L. A., & Van Vactor, D. (2009). The trip of the tip: understanding the growth cone machinery. *Nature Reviews. Molecular Cell Biology*, *10*(5), 332–343. https://doi.org/10.1038/nrm2679
Molotkov, D., Zobova, S., Arcas, J. M., & Khiroug, L. (2013). Calcium-induced outgrowth of astrocytic peripheral processes requires actin binding by Profilin-1. *Cell Calcium*, *53*(5–6), 338–348. https://doi.org/10.1016/j.ceca.2013.03.001
Moye, S. L., Diaz-Castro, B., Gangwani, M. R., & Khakh, B. S. (2019). Visualizing astrocyte morphology using lucifer yellow iontophoresis. *Journal of Visualized Experiments*, (151), 1–10. https://doi.org/10.3791/60225
Nakagawa, H., Suzuki, H., Machida, S., Suzuki, J., Ohashi, K., Jin, M., Miyamoto, S., & Terasaki, A. G. (2009). Contribution of the LIM domainand nebulin-repeatsto the interaction of Lasp-2 with actin filaments and focal

adhesions. *PLoS ONE*, *4*(10), 8–13. https://doi.org/10.1371/journal.pone.0007530
Oberheim, N. A., Takano, T., Han, X., He, W., Lin, J. H. C., Wang, F., Xu, Q., Wyatt, J. D., Pilcher, W., Ojemann, J. G., Ransom, B. R., & Goldman, S. A. (2009). Uniquely Hominid Features of Adult Human Astrocytes. *Journal of Neuroscience, 29*(10), 3276–3287. https://doi.org/10.1523/JNEUROSCI.4707-08.2009
Octeau, J. C., Chai, H., Jiang, R., Bonanno, S. L., Martin, K. C., & Khakh, B. S. (2018). An Optical Neuron-Astrocyte Proximity Assay at Synaptic Distance Scales. *Neuron*, *98*(1), 49-66.e9. https://doi.org/10.1016/j.neuron.2018.03.003
Ohta, K., Higashi, R., Sawaguchi, A., & Nakamura, K. ichiro. (2012). Helical arrangement of filaments in microvillar actin bundles. *Journal of Structural Biology*, *177*(2), 513–519. https://doi.org/10.1016/j.jsb.2011.10.012
Panda, S. K., & McGrew, M. J. (2022). Genome editing of avian species: implications for animal use and welfare. *Laboratory Animals*, *56*(1), 50–59. https://doi.org/10.1177/0023677221998400
Riedl, J., Crevenna, A. H., Kessenbrock, K., Yu, J. H., Neukirchen, D., Bista, M., Bradke, F., Jenne, D., Holak, T. A., Werb, Z., Sixt, M., & Wedlich-Soldner, R. (2008). Lifeact: a versatile marker to visualize F-actin. *Nature Methods, 5*(7), 605–607. https://doi.org/10.1038/nmeth.1220
Saint-Martin, M., & Goda, Y. (2022). Astrocyte–synapse interactions and cell adhesion molecules. *FEBS Journal*, *290*(14), 1–15. https://doi.org/10.1111/febs.16540
Saura, J. (2007). Microglial cells in astroglial cultures: A cautionary note. *Journal of Neuroinflammation*, *4*, 1–11. https://doi.org/10.1186/1742-2094-4-26
Schacke, S., Kirkpatrick, J., Stocksdale, A., Bauer, R., Hagel, C., Riecken, L. B., & Morrison, H. (2022). Ezrin deficiency triggers glial fibrillary acidic protein upregulation and a distinct reactive astrocyte phenotype. *Glia*, *70*(12), 2309–2329. https://doi.org/10.1002/glia.24253
Schiweck, J., Eickholt, B. J., & Murk, K. (2018). Important shapeshifter: Mechanisms allowing astrocytes to respond to the changing nervous system during development, injury and disease. *Frontiers in Cellular Neuroscience*, *12*(August), 1–17. https://doi.org/10.3389/fncel.2018.00261
Semyanov, A., & Verkhratsky, A. (2021). Astrocytic processes: from tripartite synapses to the active milieu. *Trends in Neurosciences*, *44*(10), 781–792. https://doi.org/10.1016/j.tins.2021.07.006
Shigetomi, E., Patel, S., & Khakh, B. S. (2016). Probing the Complexities of Astrocyte Calcium Signaling. *Trends in Cell Biology*, *26*(4), 300–312. https://doi.org/10.1016/j.tcb.2016.01.003
Smith, J., Alfieri, J. M., Anthony, N., Arensburger, P., Athrey, G. N., Balacco, J., Balic, A., Bardou, P., Barela, P., Bigot, Y., Blackmon, H., Borodin, P. M., Carroll, R., Casono, M. C., Charles, M., Cheng, H., Chiodi, M., Cigan, L., Coghill, L. M., … Zhou, H. (2023). Fourth Report on Chicken Genes and Chromosomes 2022. *Cytogenetic and Genome Research*, *162*(8–9), 405–528. https://doi.org/10.1159/000529376
Smith, M. A., Hoffman, L. M., & Beckerle, M. C. (2014). LIM proteins in actin cytoskeleton mechanoresponse. *Trends in Cell Biology*, *24*(10), 575–583. https://doi.org/10.1016/j.tcb.2014.04.009
Soto, J. S., Jami-Alahmadi, Y., Chacon, J., Moye, S. L., Diaz-Castro, B., Wohlschlegel, J. A., & Khakh, B. S. (2023). Astrocyte–neuron subproteomes and obsessive–compulsive disorder mechanisms. *Nature* (Vol. 616, Issue 7958). Springer US. https://doi.org/10.1038/s41586-023-05927-7
Soto, J. S., Neupane, C., Kaur, M., Pandey, V., Wohlschlegel, J. A., & Khakh, B. S. (2024). Astrocyte Gi-GPCR signaling corrects compulsive-like grooming and anxiety-related behaviors in Sapap3 knockout mice. *Neuron, 112*. https://doi.org/10.1016/j.neuron.2024.07.019
Svitkina, T. (2018). The actin cytoskeleton and actin-based motility. *Cold Spring Harbor Perspectives in Biology*, *10*(1). https://doi.org/10.1101/cshperspect.a018267
Terasaki, A. G., Suzuki, H., Nishioka, T., Matsuzawa, E., Katsuki, M., Nakagawa, H., Miyamoto, S., & Ohashi, K. (2004). A novel LIM and SH3 protein (lasp-2) highly expressing in chicken brain. *Biochemical and Biophysical Research Communications*, *313*(1), 48–54. https://doi.org/10.1016/j.bbrc.2003.11.085
Thomason, E. J., Escalante, M., Osterhout, D. J., & Fuss, B. (2020). The oligodendrocyte growth cone and its actin cytoskeleton: A fundamental element for progenitor cell migration and CNS myelination. *Glia*, *68*(7), 1329–1346. https://doi.org/10.1002/glia.23735
Torres-Ceja, B., & Olsen, M. L. (2022). A closer look at astrocyte morphology: Development, heterogeneity, and plasticity at astrocyte leaflets. *Current Opinion in Neurobiology*, *74*, 102550. https://doi.org/10.1016/j.conb.2022.102550
Tsukuda, S., Tamura, A., Matsumoto, K., Fujita, Y., Nakata, S., Kaneko, T., Nakayama, A., Nakagawa, H., & Terasaki, A. G. (2019). In vitro differentiation of chicken astrocytes: Growth, morphology, and protein expression of astrocytes in primary cultures. *Zoological Science*, *36*(6). https://doi.org/10.2108/zs180102
Wilson, D. M., Cookson, M. R., Van Den Bosch, L., Zetterberg, H., Holtzman, D. M., & Dewachter, I. (2023). Hallmarks of neurodegenerative diseases. *Cell*, *186*(4), 693–714. https://doi.org/10.1016/j.cell.2022.12.032
Yu, X., & Khakh, B. S. (2022). SnapShot: Astrocyte interactions. *Cell*, *185*(1), 220-220.e1.

https://doi.org/10.1016/j.cell.2021.09.029
Zieseniss, A., Terasaki, A. G., & Gregorio, C. C. (2008). Lasp-2 expression, localization, and ligand interactions: A new Z-disc scaffolding protein. *Cell Motility and the Cytoskeleton*, *65*(1), 59–72. https://doi.org/10.1002/cm.20244

Fig.1

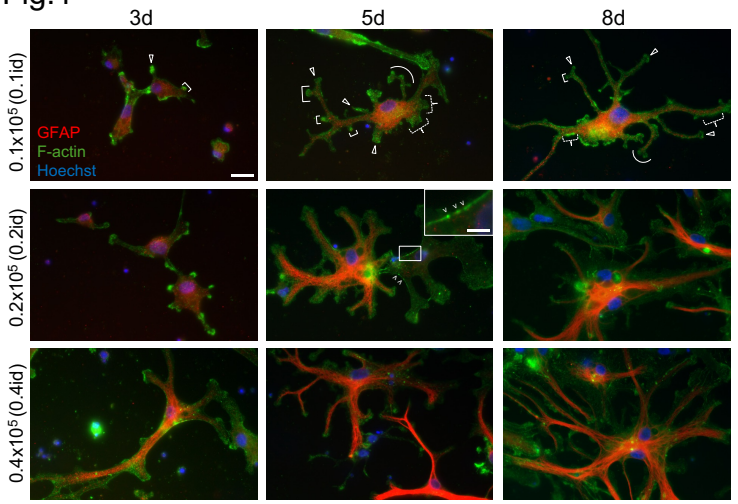
3d
5d
8d
0.1x10^5 (0.1id)
0.2x10^5 (0.2id)
0.4x10^5 (0.4id)
GFAP
F-actin
Hoechst

Fig.2

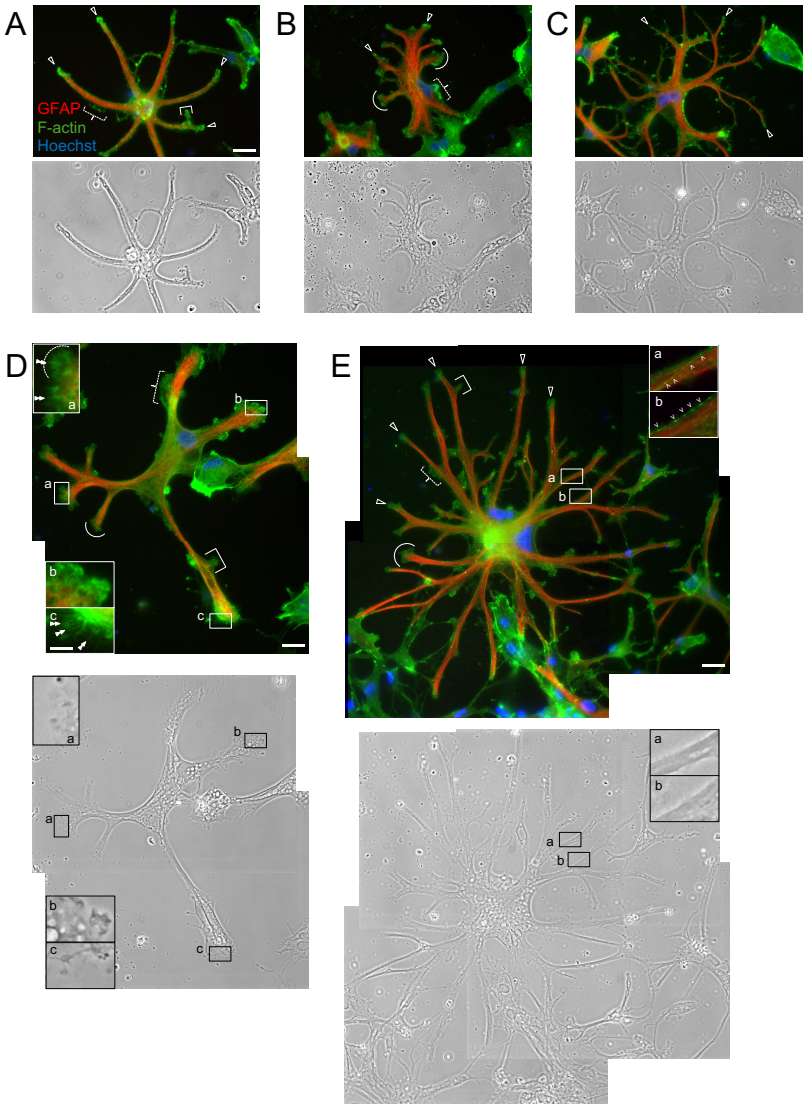

Fig.3

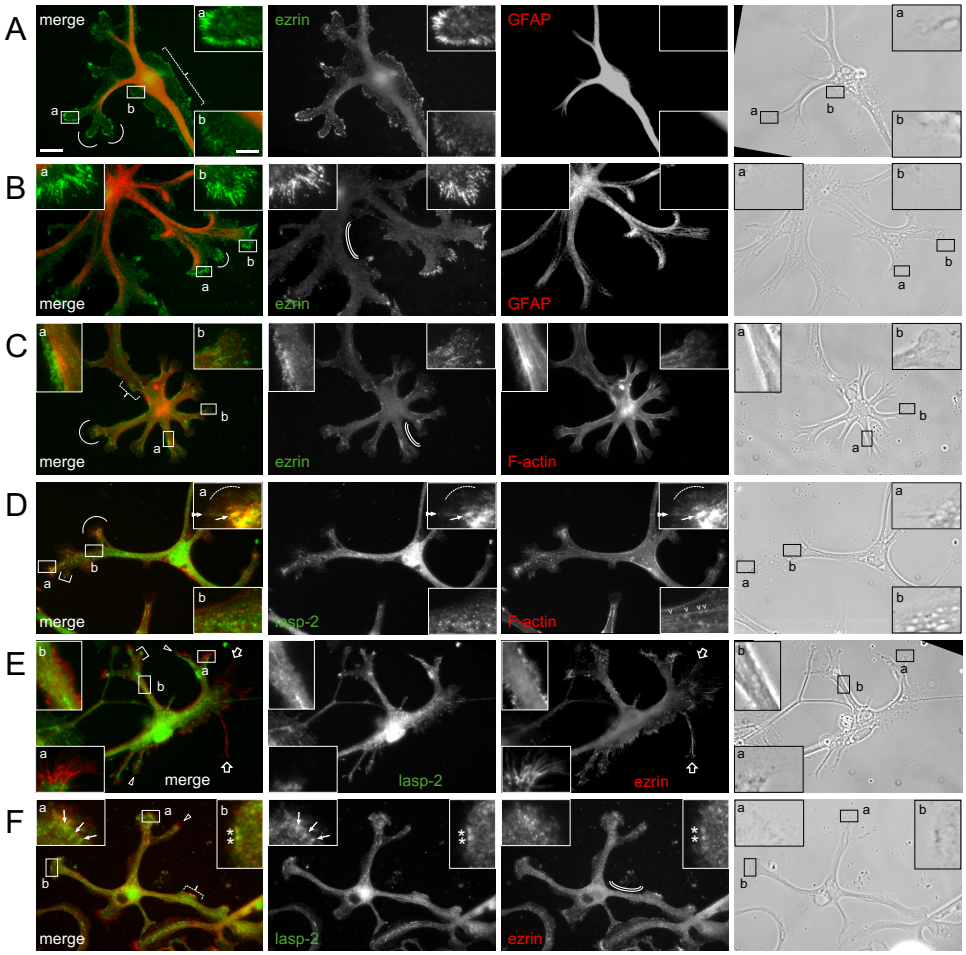
A
merge
ezrin
GFAP
B
merge
ezrin
GFAP
C
merge
ezrin
F-actin
D
merge
lasp-2
F-actin
E
merge
lasp-2
ezrin
F
merge
lasp-2
ezrin

Fig.4

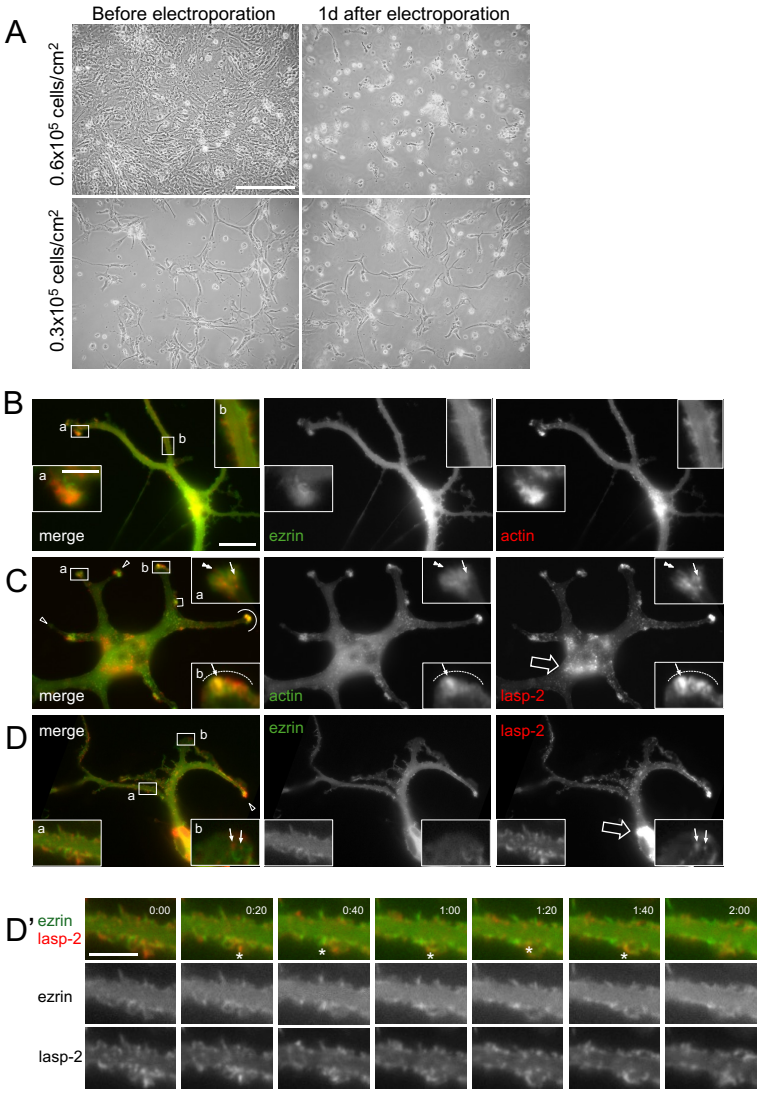
A
Before electroporation
1d after electroporation
0.6x10^5 cells/cm^2
0.3x10^5 cells/cm^2
B
merge
ezrin
actin
C
merge
actin
lasp-2
D
merge
ezrin
lasp-2
D'
ezrin
lasp-2
0:00
0:20
0:40
1:00
1:20
1:40
2:00
ezrin
lasp-2

Fig.5

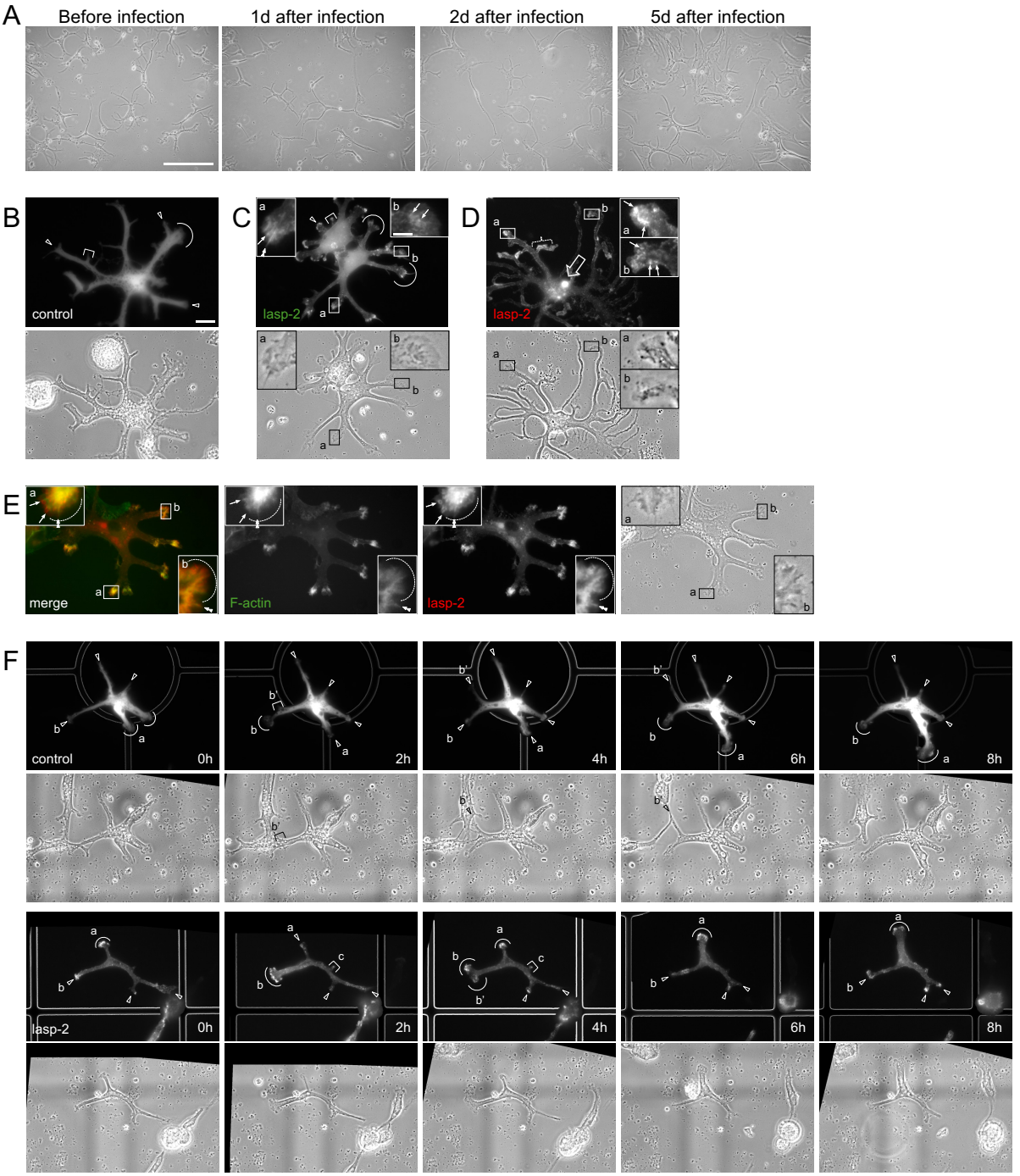
A
Before infection
1d after infection
2d after infection
5d after infection
B
control
C
lasp-2
D
lasp-2
E
merge
F-actin
lasp-2
F
control
0h
2h
4h
6h
8h
lasp-2
0h
2h
4h
6h
8h